On the size-regulation of RNA-loaded lipid nanoparticles synthesized by microfluidic device

Kento Okuda[1] †, Yusuke Sato[1] †*, Kazuki Iwakawa[1], Kosuke Sasaki[1], Nana Okabe[1], Masatoshi Maeki[2,3], Manabu Tokeshi[2,4,5], Hideyoshi Harashima[1]**

[1]Laboratory for Molecular Design of Pharmaceutics, Faculty of Pharmaceutical Sciences, Hokkaido University, Kita-12, Nishi-6, Kita-Ku, Sapporo 060-0812, Japan.

[2]Division of Applied Chemistry, Faculty of Engineering, Hokkaido University, Kita-13, Nishi-8, Kita-Ku, Sapporo 060-8628, Japan.

[3]JST PRESTO, 4-1-8 Honcho, Kawaguchi, Saitama, 332-0012, Japan

[4]Innovative Research Center for Preventive Medical Engineering, Nagoya University, Furo-cho, Chikusa-ku, Nagoya 464-8601, Japan

[5]Institute of Nano-Life Systems, Institutes of Innovation for Future Society, Nagoya University, Furo-cho, Chikusa-ku, Nagoya 464-8601, Japan

† These authors contributed equally to this work.

**Corresponding authors:*
Yusuke Sato E-mail address: y_sato@pharm.hokudai.ac.jp Tel: +81 11 706 3734 Fax: +81 11 706 3734
Hideyoshi Harashima E-mail address: harasima@pharm.hokudai.ac.jp Tel: +81 11 706 3919 Fax: +81 11 706 4879

Key words
size-regulation; DLVO theory; Hofmeister series; RNA delivery; lipid nanoparticles; microfluidic device

Abstract

The use of lipid nanoparticles (LNPs) for nucleic acid delivery is now becoming a promising strategy with a number of clinical trials as vaccines or as novel therapies against a variety of genetic and infectious diseases. The use of microfluidics for the synthesis of the LNPs has attracted interest because of its considerable advantages over other conventional synthetic methods including scalability, reproducibility, and speed. However, despite the potential usefulness of large particles for nucleic acid delivery to dendritic cells (DCs) as a vaccine, the particle size of the LNPs prepared using microfluidics is typically limited to approximately from 30 to 100 nm. In this study, focusing on Derjaguin-Landau-Verwey-Overbeek (DLVO) theory, the effect of some synthetic parameters, including total flow rate, flow rate ratio, buffer pH, lipid concentration, molar ratio of PEG-lipid as well as salt concentration, on particle size was systematically examined by means of the design of experiment approaches. The findings indicated that the simple addition of salt (*e.g.* NaCl) to a buffer containing nucleic acids contributed greatly to the synthesis of large LNPs over 200 nm and this effect was concentration-dependent with respect to the salt. The effect of salt on particle size was consistent with a Hofmeister series. The systemic injection of larger mRNA-loaded LNPs resulted in a higher transgene expression in mouse splenic DCs, a higher activation of various splenic immune cells, and had a superior effect as a therapeutic cancer vaccine in a syngeneic mouse model compared to the smaller-sized counterpart with constant lipid composition prepared with lower NaCl concentration. Collectively, size-regulation by the simple addition of salt is a promising strategy for developing potent LNPs.

1. Introduction

RNAs including short interfering RNAs (siRNAs) and mRNAs represent a promising approach for the treatment of various refractory diseases including genetic diseases, infectious diseases, and cancer, because the phenotypes of these diseases would be derived from an abnormality (upregulation, downregulation, mutations, and deletions) in genetic status [1, 2]. Despite their great potential, the unique characterization of the RNAs, including ease of enzymatic degradation in biological fluids, poor pharmacokinetics and biodistribution, severely hinders their use in *in vivo* conditions. The use of lipid nanoparticles (LNPs) for nucleic acid delivery is recognized as a promising strategy with a large number of clinical pipelines as vaccines or novel therapies against a variety of genetic and infectious diseases [3, 4]. For example, Onpattro, the first-ever siRNA medicine developed by Alnylam pharmaceuticals, is siRNA-loaded LNPs that target a transthyretin (TTR) gene expressed in hepatocytes and is used for the treatment of polyneuropathy of hereditary TTR-mediated (hATTR) amyloidosis [5]. In addition, both Comirnaty® (Pfizer/BionTech) and Spikevax® (Moderna) are the first mRNA vaccines against the current corona virus diseases 2019 (COVID-19) that were developed for the treatment of infections caused by the severe acute respiratory syndrome coronavirus 2 (SARS-CoV-2) [4, 6].

RNA-loaded LNPs are typically composed of 4 lipid components that typically include a pH-sensitive cationic lipid (CL), a phospholipid (PL), cholesterol (chol), and a polyethyleneglycol (PEG)-lipid. The pH-sensitive cationic lipids are electrostatically near neutral at physiological pH and adopt cationic properties at an acidic pH. This property allows the enhanced encapsulation of highly negatively charged RNAs in the LNPs through electrostatic interactions in an acidic buffer, thereby avoiding non-specific interactions with serum components after intravenous administration. This, in turn, facilitates rapid hepatic uptake and enhances the cytosolic delivery of RNAs through electrostatic interactions followed by fusion with endosomal membranes [7-9]. The development of potent pH-sensitive cationic lipids has been a major breakthrough in the field of LNP-based RNA delivery [10-12]. The rational design of pH-sensitive cationic lipids significantly enhanced the delivery of cargoes to hepatocytes, as well as the efficiency of cytosolic release of RNAs, and tolerability [13, 14]. The gold standard for these pH-sensitive cationic lipids is DLin-MC3-DMA (MC3), which is used in the approved Onpattro [15], and both ALC-0315 and SM-102, which are used in the mRNA vaccines against the COVID-19 [4]. It is known that Onpattro and related LNPs accumulate in hepatocytes through the apolipoprotein E (ApoE)-low-density lipoprotein receptor (LDLR) pathway. A recent study reported on the ApoE-independent mRNA delivery to extra-hepatic tissues (*i.e.* lung and spleen) by altering the apparent pKa value. Further studies will be required to elucidate relationship between the uptake mechanisms and the physicochemical properties of LNPs.

Solvent injection using microfluidic devices has several advantages for the synthesis of LNPs including ease of scale-up, high reproducibility and better size-controllability compared to

conventional batch scale production methods [16-18]. In a microfluidic device, a mixture of lipids in an organic solvent (*e.g.* EtOH) and RNAs in an aqueous phase (*e.g.* weakly acidic buffer) are rapidly mixed using an appropriate micromixer, resulting in the formation of small liposome-like vesicles due to electrostatic repulsion [19]. Neutralization of the pH-sensitive cationic lipids during the purification process (*e.g.* increasing the pH by dialysis) results in the formation of an amorphous oil droplet with pH-sensitive cationic lipids in the core and allows the fusion of the small vesicles to form relatively large final LNPs [20]. In the final LNPs, RNAs are entrapped in the core which is mainly composed of pH-sensitive cationic lipids and cholesterol. The core is surrounded by a monolayer that contains both PLs and PEG-lipids, which have bulky hydrophilic moieties [21]. Increasing the concentration of PEG-lipids, which have a high interfacial area, significantly contributes to the formation of smaller final LNPs, since the surface-to-volume ratio of the LNPs theoretically increases in inverse proportion to their size due to their droplet-like structure [22-25]. PL, which has relatively larger interfacial area than other components (CL and chol), is also known to affect LNP size for the same reason [26]. In addition, several preparation parameters including lipid concentration, flow rate ratio (FRR) between the organic and aqueous solutions and total flow rate (TFR) have been recognized as critical determinants of the size of LNPs [22, 27-30].

The size of the LNP is one of the significant parameters that affect their biodistribution. For targeting hepatocytes, the size of the LNP needs to be controlled to 100 nm or less in order to be efficiently accumulated in hepatocytes by passing through the fenestrae on liver sinusoidal endothelial cells and to avoid elimination by phagocytes (*e.g.* Kupffer cells) [31, 32]. On the other hand, because it is known that macropinocytosis, which is a unique pathway characterized by the nonspecific internalization of large amounts of extracellular fluid, is constitutively active in immature dendritic cells (DCs), relatively larger sized particles (*e.g.* 200 nm or over) would be beneficial for targeting DCs [33, 34]. However, range of final size of LNPs synthesized by microfluidic devices is typically limited to 100 nm or less. Although larger LNPs can be formed in the absence of or low amounts (*e.g.* less than 0.5 mol%) of PEG-lipid, low FRR (*e.g.* 1), or low TFR, these approaches are not suitable for LNP production because these parameter settings result in a low colloidal stability, low reproducibility, inefficient (slow) production, and compositional heterogeneity [22, 35]. Therefore, a novel strategy for adjusting the sizes of LNPs over a wide range is needed.

In the present study, we focused on Derjaguin-Landau-Verwey-Overbeek (DLVO) theory, which seeks to explain colloidal dispersion stability and describes the force between charged surfaces, in controlling the sizes of RNA-loaded LNPs [36]. The effect of several synthetic parameters, including total flow rate (TFR), flow rate ratio (FRR), buffer pH, lipid concentration, molar ratio of PEG-lipid as well as salt concentration, on particle size was clarified in this study. Salt concentration had the most significant effect on particle size and the simple addition of a salt (*e.g.* NaCl) to buffer solutions of RNAs resulted in the formation of large LNPs over 200 nm and this was a concentration-dependent

process. The effect of salt on particle size clearly followed the Hofmeister series. The systemic injection of larger mRNA-loaded LNPs resulted in a higher expression of activation markers on mouse splenic lymphocytes and DCs, a higher transgene expression in splenic DCs, and exerted a superior effect as therapeutic cancer vaccines in a syngeneic mouse model compared to the smaller-sized counterparts that contained exactly the same lipid composition. These findings point to the significance of controlling LNP size to maximize both transgene expression and therapeutic efficacy.

2. Materials and Methods

2.1 Materials

The pH-sensitive cationic lipids, CL4H6, were synthesized as described previously [13]. Chol was purchased from SIGMA Aldrich (St. Louis, MO). 1,2-Distearoyl-*sn*-glycero-3-phosphocholine (DSPC), 1,2-dioleoyl-*sn*-glycero-3-phosphocholine (DOPC), 1,2-dioleoyl-*sn*-glycero-3-phosphoethanolamine (DOPE), and 1,2-dimirystoyl-*rac*-glycero, methoxyethyleneglycol 2000 ether (PEG-DMG) were obtained from the NOF Corporation (Tokyo, Japan). 3,3'-Dioctadecyloxacarbocyanine perchlorate (DiO) and Ribogreen were purchased from ThermoFisher Scientific (Waltham, MA, USA). PE Anti-mouse CD40 antibody (clone FGK45), FITC anti-mouse CD80 antibody (clone 16-10A1), PE anti-mouse CD86 antibody (clone A17199A), APC anti-mouse CD69 antibody (clone H1.2F3), PerCP/Cyanine 7 anti-mouse CD19 antibody (clone 6D5), APC anti-mouse CD11c antibody (clone N418), PerCP/Cyanine 5.5 anti-mouse I-A/I-E antibody (clone M5/114.15.2), and propidium iodide (PI) were purchased from BioLegend (San Diego, CA). Anti-human polo-like kinase 1 (hPLK1) siRNA (siPLK1, sense: 5'-AGA uCA CCC uCC UUA AAu AUU-3'; antisense; 5'-UAU UUA AGG AGG GUG AuC UUU-3'), anti-mouse factor VII (FVII) siRNA (siFVII, sense: 5'-GGA **uc**A **ucu c**AA G**uc uu**A **c**TsT-3'; antisense; 5'-G**u**A AGA **cuu** GAG A**u**G A**uc c**TsT-3'), and anti-mouse CD45 siRNA (siCD45, sense: 5'- cuG Gcu GAA uuu cAG AGc ATsT-3'; antisense; 5'-G**u**A AGA **cuu** GAG A**u**G A**uc c**TsT-3) (2'-fluoro-modified nucleotides and 2'-OMe-modified nucleotides are shown in lower bold case and in lower case, respectively. Phosphorothioate linkages represented as s.) were purchased from Hokkaido System Science Co., Ltd. (Sapporo, Japan). The ovalbumin (OVA)-encoding mRNAs was purchased from Trilink BioTechnologies. (San Diego, CA, USA). A microfluidic device, an invasive lipid nanoparticle production (iLiNP) device, was fabricated as described previously [18].

2.2 Mice and cell cultures

E.G7-OVA cells, generated by transducing the chicken OVA gene into the EL4 murine lymphoma cell line were obtained from the American Type Culture Collection (Manassas, VA). E.G7-OVA cell was grown in Roswell Park Memorial Institute (RPMI) 1640 (Sigma Aldrich, MO) supplemented with 50 μM of β-mercaptoethanol, 10% fetal calf serum, 10 mM HEPES, 1 mM sodium pyruvate and 100 Units/mL of penicillin/streptomycin. Cells were cultured at 37°C in 5% CO_2 incubator.

BALB/c mice (female, 4 week of age) and C57BL/6N mice (female, 6 weeks of age) were purchased from Japan SLC (Shizuoka, Japan). The experimental protocols were reviewed and approved by the Hokkaido University Animal Care Committee in accordance with the guidelines for the care and use of laboratory animals.

2.3 *In vitro* transcription of mRNA

Nanoluciferase (Nluc)-encoding mRNA (mNluc) was synthesized from linearized pDNA by *in vitro* transcription using an mMESSAGE mMACHINE™ T7 Transcription Kit (ThermoFisher Scientific Inc., MA, USA) according to the manufacturer's recommended protocol. The *in vitro* transcribed mRNA was purified using MEGAclear™ Transcription Clean-Up Kit (ThermoFisher Scientific Inc., MA, USA) according to the manufacturer's protocol. The purified mRNA was quantified by absorbance and was stored at -80°C until used.

2.4 Preparation and characterization of RNA-loaded LNPs

Ethanol solutions containing CL4H6, a phospholipid, chol, and PEG-DMG at the indicated molar ratios were prepared at the indicated total lipid concentration (4 to 16 mM). The RNA was dissolved in a 25 mM acetate buffer (pH4.0 to 6.0) containing 10 to 250 mM neutral salt (*e.g.* NaCl). LNPs were prepared by mixing the lipids in ethanol and RNA in an aqueous solution using an iLiNP device at a total flow rate (TFR) of 0.1 to 0.5 mL/min and a flow rate ratio (FRR) (RNA flow rate/lipid flow rate) of 3 to 9. The nitrogen to phosphate (N/P) ratio was adjusted to 10. Syringe pumps (Harvard apparatus, MA, USA or YMC Co., Ltd., Kyoto, Japan) were used to control the flow rate of the solutions. The resulting LNP solution was then dialyzed for 2 hr or more at 4°C against 20 mM MES buffer (pH6.0) followed by phosphate buffered saline without Ca^{2+} and Mg^{2+} (PBS(-)) using Spectra/Por 4 dialysis membranes (molecular weight cut-off 12,000-14,000 Da, Spectrum Laboratories, Rancho Dominguez, CA).

The ζ-average size, polydispersity index (PdI), and ζ-potential of the LNPs were measured by means of a Zetasizer Nano ZS ZEN3600 instrument (Malvern Instruments, Worchestershire, UK). The encapsulation efficiency and total concentration of mRNA were measured by a Ribogreen assay, as described previously [37].

2.5 Measurement of plasma coagulation factor VII (FVII) activity

BALB/c mice were intravenously injected with the LNPs at a dose of 0.1 mg siFVII/kg. At 24 hours after the injection, mice were euthanized, and blood was collected by cardiac puncture and processed to plasma using heparin. Plasma FVII activity was measured using a Biophen FVII chromogenic assay kit (Aniara Corporation, West Chester, OH, USA) according to manufacturer's protocol.

2.6 Measurement of cellular uptake and gene silencing activity in splenic DCs

BALB/c mice were intravenously injected with siCD45-loaded DiO-labeled LNPs at a dose of 0.5 mg siRNA/kg. Spleen tissues were then harvested, and the resulting dissociated splenocytes were passed through a cell strainer (40 μm pore, BD Falcon, CA) 24 hours after the injection. The recovered cells were spun down (400 ×g, 4°C, 5 min), the supernatant removed, and then resuspended in RBC Lysis buffer (1 mL, Biolegend) and incubated for 3 min at room temperature. These treated cells were

washed with HBSS(-) by spinning (400 ×g, 4°C, 5 min). The concentration of the cells was adjusted to 1 × 10^7 cells/mL with FACS buffer and the resulting cells were treated with a 10 μg/mL solution of an anti-mouse CD16/32 antibody followed by incubation at 4°C for 10 min, then treated with an APC anti-mouse CD11c antibody and PerCP/Cyanine5.5 anti-mouse I-A/I-E antibody at 4°C for 30 min. The resulting cells were washed twice with FACS buffer, filtered through a nylon filter, stained with PI, and applied for cell sorting (SONY SH800 cell sorter, SONY, Japan). Cellular uptake in living DCs defined as $PI^-I\text{-}A/I\text{-}E^+CD11c^+$ cells was then measured. Three to five thousand living DCs were then collected in a sample tube containing TRIzol™ LS reagent (ThermoFisher Scientific Inc.). Total RNA was purified using a PureLink™ RNA Micro Scale Kit (ThermoFisher Scientific Inc.) according to the manufacturer's protocol. The total RNA was reverse-transcribed to cDNA using ReverTra Ace qPCR RT Master Mix with gDNA Remover (TOYOBO Co., Ltd., Osaka, Japan). Quantitative PCR analysis was performed on the cDNA using the PrimeTime Gene Expression Master Mix (IDT) and the Thermal Cycler Dice® Real Time System III (TaKaRa Bio Inc., Shiga, Japan). All reactions were performed in a volume of 10 μL. The primers/probes (IDT) for mouse CD45 were (forward) 5'-TTT CCA ATG TGC TGT GTC CT-3', (reverse) 5'-TGA AGA AGA GAG ATC CAC CCA-3', and (probe) 5'-/56-FAM/ TGG AGG CTG /ZEN/ AAT ACC AGA GAC TTC CT/3IABkFQ/-3', and for mouse peptidylprolyl isomerase A (Ppia) were (forward) 5'-CAA ACA CAA ACG GTT CCC AG-3', (reverse) 5'-TTC ACC TTC CCA AAG ACC AC-3', and (probe) 5'-/56-FAM/ TGC TTG CCA /ZEN/ TCC AGC CAT TCA G/3IABkFQ/-3'.

2.6 Measurement of Nluc activity in splenic DCs

BALB/c mice were intravenously injected with mNluc-loaded LNPs at a dose of 0.2 mg mRNA/kg. Spleen tissues were harvested, and the resulting dissociated splenocytes were passed through a cell strainer (40 μm pore, BD Falcon, CA) 24 hours after the injection. The recovered cells were spun down (400 ×g, 4°C, 5 min) to remove the supernatant, resuspended in RBC Lysis buffer (1 mL, Biolegend) and incubated for 3 min at room temperature. These treated cells were washed with HBSS(-) by spinning (400 ×g, 4°C, 5 min). The concentration of the cells was adjusted to 1 × 10^7 cells/mL with FACS buffer and the resulting cells were treated with 10 μg/mL anti-mouse CD16/32 antibody and were incubated at 4°C for 10 min, then treated with an APC anti-mouse CD11c antibody and PerCP/Cyanine5.5 anti-mouse I-A/I-E antibody at 4°C for 30 min. Cells were washed with FACS buffer twice, filtered through a nylon filter, stained with PI, and applied for cell sorting (SONY SH800 cell sorter, SONY, Japan). Three thousand living DCs defined as $PI^-I\text{-}A/I\text{-}E^+CD11c^+$ cells were collected in a sample tube containing 20 μL of passive lysis buffer. Nluc activity was measured using the Nano-Glo Luciferase Assay Kit (Promega) according to manufacturer's protocol. Luminescence was measured using a luminometer (Luminescencer-PSN, ATTO, Japan). Nluc activity was expressed as relative light units (RLU) per 3,000 DCs.

2.7 Measurement of activation markers in splenocytes

BALB/c mice were intravenously injected with mOVA-loaded LNPs at a dose of 0.2 mg mRNA/kg. Spleen tissues were harvested, and the resulting dissociated splenocytes were passed through a cell strainer (40 μm pore, BD Falcon, CA) 24 hours after the injection. The recovered cells were spun down (400 ×g, 4°C, 5 min) to remove the supernatant, resuspended in RBC Lysis buffer (1 mL, Biolegend) and incubated for 3 min at room temperature. These treated cells were washed with HBSS(-) by spinning (400 ×g, 4°C, 5 min). The concentration of the cells was adjusted to 1×10^7 cells/mL with FACS buffer and the resulting cells were treated with 10 μg/mL anti-mouse CD16/32 antibody and were incubated at 4°C for 10 min, then treated with fluorophore-conjugated antibodies at 4°C for 30 min. The cells were washed with FACS buffer twice, filtered through a nylon filter, stained with propidium iodide (PI) (BioLegend), and applied for flowcytometric analysis (CytoFLEX, Beckman Coulter, Inc., CA). DCs, T cells, and B cells were defined as I-A/I-$E^+$$CD11c^+$ cells, $CD3^+CD19^-$ cells, and $CD3^-CD19^+$ cells, respectively.

2.8 Therapeutic antitumor effect of mRNA-loaded LNPs on mice

C57BL6/N mice (6 weeks old) were anesthetized with isoflurane. E.G7-OVA cells (8×10^6 cells/40 μL/mouse) were inoculated subcutaneously in the right flank. The tumor-bearing mice were intravenously injected with OVA-encoding mRNA (mOVA)-loaded LNPs at doses of 0.2 mg mRNA/kg on day 7 and 10. Tumor volumes were calculated by the following method (tumor volume = major axis × minor $axis^2$ × 0.52) from day 6 to 18.

2.9 Statistical analysis

Statistical data obtained by the DOE were analyzed using the JMP 14 software (SAS, Cary, NC, USA). Statistical significance was defined as *p*-values less than 0.05. Three independent experiments were performed for the DOE. To identify significant factors for each physicochemical property of the LNPs in a relatively vast experimental design space, 3^6 and $3^5 \times 2^1$ definitive screening designs (DSDs) were used for the screening of the preparation conditions and of LNP composition, respectively. Effective design-based model selection for DSD or the forward stepwise regression method with Akaike's information criterion and finite correction (c-AIC) was applied to each response. The forward stepwise regression method with c-AIC was applied only in cases where the number of both statistically significant main factors and interactions between 2 factors were less than 3. For examining the effect of helper lipid, a $4^1 \times 2^2$ full factorial design (FFD) was used. A standard least squares linear regression model was applied to each response.

Results are expressed as the mean + SD or the mean ± SD of independent repeats. For comparisons between the means of two variables, we used unpaired Student's *t* tests. For comparisons between multiple groups, we used one-way ANOVA with the Student–Newman–Keuls *post hoc* test.

3. Results and discussion

3.1 Strategy for controlling LNP size based on DLVO theory

In this study, a microfluidic device, iLiNP device, was used to achieve a reproducible preparation of RNA-loaded LNPs (Figure 1A). Baffle structures of the iLiNP device generates a secondary flow in a microchannel, which results in efficient (in the millisecond order) mixing performance at a high flow rate [18]. This leads to rapid nucleation and minimizing particle growth by Ostwald ripening, resulting in the reproducible production of homogenous LNPs. On the other hand, producing homogenous and large LNPs (>100 nm in diameter) is relatively challenging. A lower total flow rate (TFR) results in the formation of large and LNPs with heterogenous size distribution due to the consumption of lipids for nuclear growth [38]. It also leads to lower production rate. Lower amounts of PEG-lipid with high interfacial areas also results in producing large LNPs because total interfacial area of the LNPs decreases with increasing size [23, 24]. An appropriate amount of PEG-lipid is required for achieving both colloidal stability during storage and acceptable pharmacokinetics (*e.g.* blood half-life). Therefore, alternative approaches for controlling size with reasonable conditions (*e.g.* a high production rate, inexpensive, non-toxic) is desired. Kulkarni *et al.* reported that ultra-small and unstable cationic liposome-like particles are initially formed due to electrostatic repulsion between cationic lipids [19]. These cationic liposome-like particles would be hydrophobic cationic colloids because the interfacial PEG density is low due to their high total interfacial area. After subsequent neutralizing the cationic liposome-like particles (*e.g.* dilution with or dialysis against PBS or other neutral buffer), the particles grow to equilibrium size through fusion [19, 20]. Considering the formation process, we focused on the initially formed cationic liposome-like particles, which are hydrophobic cationic colloids. We hypothesized that it would be possible to control the final LNP size by modulating the colloidal stability of the hydrophobic cationic colloids. To achieve this, we focused on DLVO theory regarding the stability of hydrophobic colloids based on interactions between electrical double layers of the adjacent colloids (Figure 1B). The total potential energy (V_{total}) is expressed as the sum of the interaction energies by electrostatic repulsion (V_R) and London-van der Waals attraction (V_A). When the V_{total} value is low or negative, colloids are in general agglomerated or aggregated in an uncontrollable manner. However, in the case of LNPs, the interfacial PEG density become higher as the cationic liposome-like particles increase in size, which inhibits further aggregation. Therefore, it would be expected that particle size can be regulated by modifying the V_{total} by changing manufacturing conditions. The V_{total} is expressed by the formula shown in Figure 1B where ψ_0, k, e, and A are the surface potential, the Boltzmann constant, elementary charge, and the Hamaker constant, respectively, and these are all constant values. The terms a, H, $\varepsilon_r\varepsilon_0$, n, z, and T are particle size, distance between particles, permittivity, ion concentration, ion valence, and absolute temperature, respectively, and these can be controlled by manipulating the formulation conditions. For example, a higher FRR results in $\varepsilon_r\varepsilon_0$ being lower because the relative permittivity of EtOH and water

are 24.3 and 78.3, respectively. This results in a lower V_R and therefore a lower V_{total}, leading to particle growth. The addition of a salt (*e.g.* NaCl) in the buffer results in a higher n, a lower V_R and therefore a lower V_{total}, leading to particle growth. A buffer with a higher pH leads to a lower ψ_0 when LNPs are composed of a pH-sensitive cationic lipid, which would be electrostatically near neutral at physiological pH (*e.g.* pH 7.4), thus resulting in a particle with cationic properties under a weakly acidic pH (*e.g.* pH 5), resulting in a lower V_R and therefore a lower V_{total}, leading to particle growth. A higher lipid concentration leads to a decrease in the H, which results in an increase in both V_R and V_A. Therefore, its effect on V_{total} would be affected by other variables such as $\varepsilon_r\varepsilon_0$ and so on. A higher FRR would also lead to a decrease in the H because it refers to the dilution rate of the lipid components. A higher a also results in an increase in both V_R and V_A. A higher T leads to an increase in V_R and therefore a higher V_{total}. However, it was not possible for us to control or precisely change the temperature during the operation due to limitations of our laboratory equipment. All of the LNPs were synthesized at room temperature in this study, and therefore, fluctuations in room temperature between experiments could potentially contribute to increased errors in the sizes of the LNPs. Although the TFR would not be related to DLVO theory directly, a decrease results in the formation of large and heterogenous LNPs due to the consumption of lipids for nuclear growth [38].

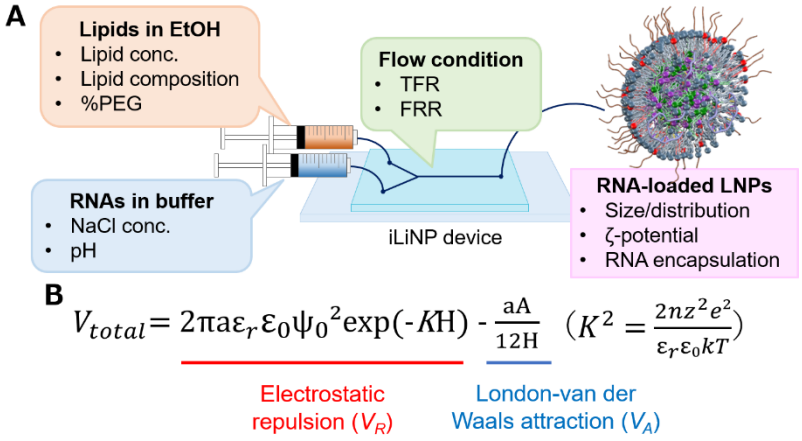

Figure 1. Physicochemical properties of RNA-loaded LNPs are related to formulation parameters. (A) Schematic illustration of the synthesis of RNA-loaded LNPs using a microfluidic device, formulation parameters and physicochemical properties of the LNPs examined in this study. (B) Formula representing DLVO theory.

3.2 Effect of preparation conditions on the physicochemical properties of the LNPs

DOE was used to understand the effect of formulation parameters on the physicochemical properties of RNA-loaded LNPs in a systematic manner. In the 1st DOE, LNPs composed of CL4H6, DOPE, cholesterol, and PEG-DMG at molar ratio of 50/10/40/x were used, and 6 independent formulation

parameters including TFR (level: 100 to 500 μL/min), FRR (level: 3 to 9), NaCl concentration in buffer (NaCl conc.) (level: 10 to 250 mM), molar percentage of PEG-DMG (%PEG) (level: 1 to 2 mol%), total lipid concentration (Lipid conc.) (level: 4 to 16 mM), and pH of buffer (level: 4 to 6), were systematically examined by 3^6 DSD to identify significantly contributing factor(s) with minimal confounding with two-factor interactions (Table 1). In this study, the nitrogen per phosphate (N/P) ratio was fixed at 10. The siRNA-loaded LNPs were synthesized under 17 different formulation conditions (coded as A1 to A17) that were determined based on DSD. The diameters of the LNPs varied with a ζ-average from 60 to 260 nm (Figure 2A) or a number mean from 41 to 171 nm (Figure S1) with low (< 0.2) PdI (Figure 2B), slightly negative to near neutral (-8 to 4 mV) (Figure 2C), and a moderate to high encapsulation efficiency (74 to 96%) (Figure 2D) depending on formulation conditions. Concerning diameter, a well-fitted regression model (R^2=0.996) was obtained by the effective design-based model selection for DSD (Figure 2E, S2). All 6 factors that were examined in this experiment were found to significantly contribute to the size of the LNPs. The concentration of NaCl was the most significant factor and its increase resulted in the formation of larger LNPs. This finding was reasonable because the salt concentration was estimated to have the highest impact on V_R changes due to the wide range of the level compared to other factors. It should also be noted that the range of levels for other factors were not intentionally narrow and are limited for the following reasons: lower (< 100 μL/min) and higher TFR (> 500 μL/min) lead to inefficient (slow) production and the above pressure limit, lower (< 3) and higher FRR (> 9) leads to reduced reproducibility due to nuclear growth and unnecessary dilution, lower (< 4) and higher pH (> 6) leads to acid hydrolysis of some of the components (lipids and RNAs) and an inefficient encapsulation of RNAs through electrostatic interactions because the pKa of the pH-sensitive cationic lipid used in this study is 6.25 [13], a lower (< 4 mM) lipid concentration leads to difficult particle formation, and lower (< 1) and higher (> 2) %PEG leads to lower stability during storage and the formation of unnecessarily small particles, respectively. The other 5 factors showed roughly similar contributions. A decrease in TFR, FRR, and %PEG, and an increase in lipid concentration and pH resulted in the formation of larger LNPs. These contributions were in good agreement with our predictions based on DLVO theory as described above. In addition, the FRR interacted with other factors (*i.e.* pH, NaCl conc., and TFR) possibly due to its effect on both H and $\varepsilon_r\varepsilon_0$. Although a well-fitted regression model was successfully obtained, the model predicted that LNPs would be formed with an unachievable small size (*e.g.* less than 20 nm) in a few cases (Figure S3), suggesting the potential limitations of linear regression or a small number of experiments compared to a large experimental space (17 out of 729). The addition of some different formulation conditions and/or applying non-linear regression models are potential candidates for improving prediction accuracy. The concentration of NaCl also contributed to a decrease in siRNA encapsulation (Figure S4), and this point is discussed below. The stability of the siRNA-loaded LNPs synthesized under different conditions were evaluated. The physicochemical properties of A2-, A5-,

and A14-LNPs were measured after storage at 4°C as a wet preparation for up to 2 weeks. Although a slight increase and decrease in size and encapsulation were observed for A5- and A14-LNPs, no correlation between initial size and stability during storage was observed (Figure S5). Since the stability of the LNPs during storage depends on a variety of parameters (*e.g.* chemical structure, lipid composition, buffer condition, among others), further optimization from the viewpoint of stability would be necessary as a separate study.

Table 1. A list of formulations (A1 to A17) for examining formulation parameters determined based on DSD

Entry	TFR (μL/min)	FRR	NaCl conc. (mM)	%PEG	Lipid conc. (mM)	pH
A1	100	6	10	1	16	4
A2	100	3	10	2	4	6
A3	100	9	10	2	16	5
A4	100	9	130	1	4	6
A5	100	3	250	1	16	6
A6	100	9	250	1.5	4	4
A7	100	3	250	2	10	4
A8	300	3	10	1	4	4
A9	300	6	130	1.5	10	5
A10	300	9	250	2	16	6
A11	500	9	10	1	10	6
A12	500	3	10	1.5	16	6
A13	500	9	10	2	4	4
A14	500	3	130	2	16	4
A15	500	6	250	2	4	6
A16	500	3	250	1	4	5
A17	500	9	250	1	16	4

To confirm utility of this process related to formulation conditions, siFVII-loaded LNPs (coded as B1 to B5) were synthesized under 5 different conditions (Table 2). The size of the LNPs were adjusted to a specific range from 100 to 120 nm by using the regression model because it is known to affect RNA delivery. All of the LNPs showed consistent and high encapsulation efficiency (Table 2). Mice were intravenously injected at 0.1 mg siRNA/kg. All of the LNPs showed substantial FVII gene silencing, but only the B1-LNPs showed significantly lower gene silencing activity compared to the

others (Figure 2F). This can be attributed to the formation of compositionally heterogenous particles due to a lower TFR. On the other hand, 4 of the LNPs (B2 to B5) showed better gene silencing activity, suggesting that the formulation conditions that were examined, except for the lower TFR, would be useful for controlling the size of LNPs for RNA delivery. We also measured the VII gene silencing activity of 4 different-sized LNPs (ζ-average from 76 to 229 nm) prepared under different NaCl concentrations from 10 to 370 mM. No significant difference in gene silencing activity was observed between the 4 LNPs (Figure S6), suggesting that at least the addition of NaCl to the siRNA solution has no negative affect on gene silencing activity, which is consistent with the data shown in Figure 2F. It is known that the average size and size distribution of mouse fenestrae are higher than the corresponding values for other species including humans and rabbits [39]. Therefore, this size range would not be expected to have a significant impact on gene silencing activity in hepatocytes. A similar observation was made in our previous study [31].

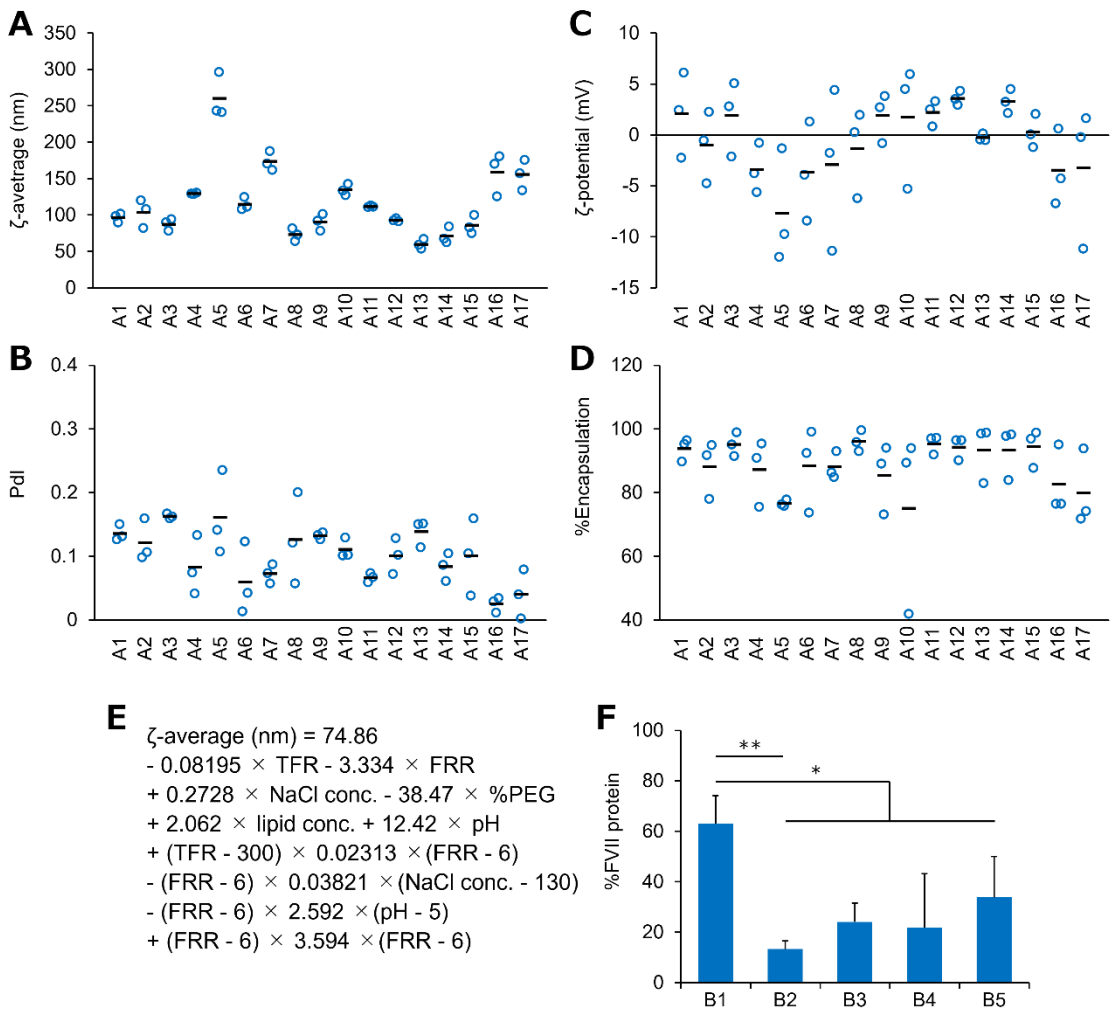

Figure 2. Physicochemical properties of the siRNA-loaded LNPs (A1 to A17). (A-D) ζ-

Average (A), PdI (B), ζ-potential (C), and percentage of siRNA encapsulation (D) of the LNPs. n=3. (E) A regression equation for the size of siRNA-loaded LNPs determined by the DOE. (F) Plasma FVII protein levels after intravenous injection of siFVII-loaded B1- to B5-LNPs. n=3-8. *p<0.05, **p<0.01.

Table 2. A list of formulation parameters and physicochemical properties of the siRNA-loaded LNPs (B1 to B5) (n=4).

Entry	TFR (μL/min)	FRR	NaCl conc. (mM)	%PEG	lipid conc. (mM)	pH	ζ-average (nm)	Number mean (nm)	PdI	ζ-potential (mV)	%Encapsulation
B1	100	3	100	1.5	10	4	103±6	79±7	0.08±0.02	2.7±0.9	95.6±0.4
B2	500	9	10	1	10	6	113±6	91±9	0.07±0.02	3.5±0.7	94.7±1.3
B3	500	3	250	2	10	4	117±10	94±10	0.06±0.02	2.2±1.3	96.3±0.9
B4	500	6	130	1.5	10	6	123±10	91±8	0.08±0.01	2.8±0.7	95.4±0.8
B5	300	6	250	2	10	6	119±11	80±8	0.13±0.02	2.7±1.1	95.2±2.0

3.3 Effect of the composition of the LNPs on physicochemical properties

We next systematically examined the effect of lipid composition, including the molar percentage of CL (%CL) (level: 40 to 60), the molar percentage of PL (%PL) (level: 10 to 20), %PEG (level: 1 to 2), a type of PL, N/P ratio (4 to 10), and the concentration of NaCl (level: 10 to 250). The TFR, FRR, lipid concentration and pH were fixed at 500 μL/min, 3, 16 mM, and 4, respectively. To determine the effect of the structure of PL, we used 3 types of PL samples, including DOPC, DOPE, and DSPC (DOPE and DSPC have the same or different scaffolds and a different or the same head group with DOPC, respectively). In this study, we adopted DSD to minimize confounding with two-factor interactions. Two $3^5 \times 2^1$ DSDs (DOPC vs DOPE or DSPC) were merged due to limitations in DSD and the number of levels for categorical factor is only 2. Based on the merged DSD, 27 different LNPs (coded as C1 to C27) were synthesized (Table 3). The diameters of the LNPs were from 46 to 237 nm, low PdI (< 0.2), mostly near neutral but slightly negative in two cases (C6 and C9), and a moderate to high encapsulation efficiency (60 to 100%) (Figure 3 and S7). The concentration of NaCl was the most dominant determinant for the size of LNPs (Figure S7A, S8 and S9). The %PEG was also a significant factor. On the other hand, the % and type of PL had no effect on LNP size. Increasing the concentration of NaCl Resulted in a significant decrease in encapsulation efficiency (Figure S10 and S11). DOPC showed a significantly lower encapsulation efficiency compared to both DOPE and DSPC especially in case where the concentration of NaCl was high.

Table 3. A list of formulations (C1 to C27) used for examining formulation parameters determined based on DSD.

Entry	%CL	%PL	%PEG	N/P ratio	NaCl conc. (mM)	PL
C1	40	10	1	10	10	DOPC
C2	40	20	1.5	4	10	DOPC
C3	60	15	2	10	10	DOPC
C4	60	10	2	4	10	DOPC
C5	50	15	1.5	7	130	DOPC
C6	60	20	1	4	130	DOPC
C7	40	10	2	4	250	DOPC
C8	50	20	2	10	250	DOPC
C9	60	10	1	7	250	DOPC
C10	40	20	2	7	10	DOPE
C11	50	10	1	4	10	DOPE
C12	60	20	1	10	10	DOPE
C13	40	10	2	10	130	DOPE
C14	50	15	1.5	7	130	DOPE
C15	40	20	1	10	250	DOPE
C16	40	15	1	4	250	DOPE
C17	60	20	2	4	250	DOPE
C18	60	10	1.5	10	250	DOPE
C19	40	20	2	7	10	DSPC
C20	50	10	1	4	10	DSPC
C21	60	20	1	10	10	DSPC
C22	40	10	2	10	130	DSPC
C23	50	15	1.5	7	130	DSPC
C24	40	20	1	10	250	DSPC
C25	40	15	1	4	250	DSPC
C26	60	20	2	4	250	DSPC
C27	60	10	1.5	10	250	DSPC

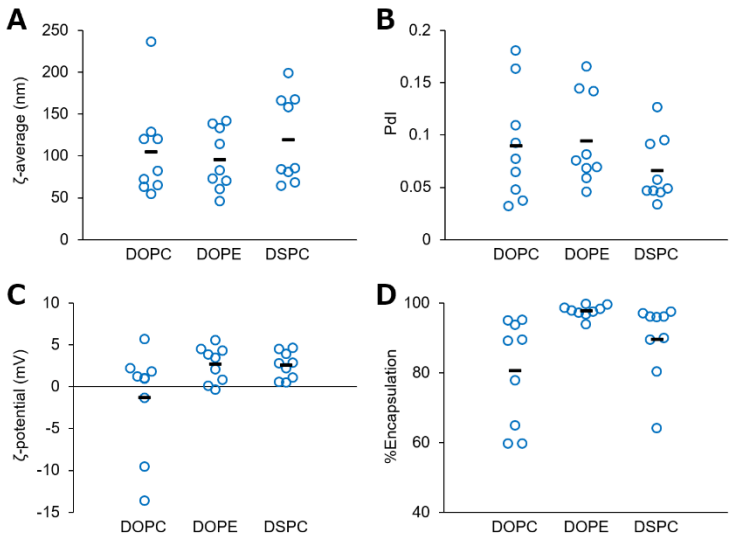

Figure 3. Physicochemical properties of the siRNA-loaded LNPs (C1 to C27). ζ-Average (A), PdI (B), ζ-potential (C), and percentage of siRNA encapsulation (D) of the LNPs. n=3.

A $4^1 \times 2^2$ full factorial design (FFD) was then performed to collect additional, more precise information on the effect of helper lipids on encapsulation efficiency. In this study, LNPs with a fixed lipid composition (CL4H6/X/cholesterol/PEG-DMG=50/15/35/1.5 mol%, N/P ratio: 7) were synthesized by formulation conditions involving a fixed TFR (500 μL/min), varied FRR (3 or 9), a fixed lipid concentration (16 mM), and varied concentrations of NaCl (130 or 250 mM). The X in the lipid composition indicates a following helper lipid: DOPC, DOPE, DSPC, and cholesterol (no PL). An increase in in the concentration of NaCl again resulted in the formation of larger LNPs without significant dependence on the type of helper lipid (Figure 4A and S12). All of the LNPs were uniform (PdI < 0.2) (Figure 4B). On the other hand, the helper lipid clearly had an effect on encapsulation efficiency and ζ-potential (Figure 4C and 4D). Only DOPE showed a consistently high (97%) encapsulation efficiency, and the other helper lipids showed lower encapsulation efficiency depending on concentration of NaCl. The order of encapsulation efficiency is as follows: DOPC < cholesterol < DSPC < DOPE. DSPC, which is composed of saturated stearyl (C18:0) scaffolds, shows a higher van der Waals attraction and therefore higher stabilized lipid membranes compared to DOPC, which is composed of unsaturated oleyl (C18:1) scaffolds. Although NaCl can compete with electrostatic interactions between RNAs and CLs, the interaction between RNA and the CL-containing membrane would be strong due to multivalent effects. However, the difference in encapsulation efficiency between DOPC and DSPC suggest that the fluidity or stability of the CL-containing membrane is important in terms of the concentration of NaCl. DOPC potentially shows a higher solubility in EtOH-containing buffer due to lower hydrophobic interactions compared to DSPC. Therefore, DOPC-containing LNPs were potentially more soluble under formulation conditions with an FRR of 3 (EtOH

conc.: 25%). To avoid the potential contribution of solubility, an FRR of 9 (EtOH conc.: 10%) was also performed. No significant change in encapsulation efficiency was observed for DOPC-containing LNPs at a NaCl concentration of 250 mM (Figure 4D), suggesting that membrane fluidity but not lipid solubility is involved in the competition by NaCl. DOPE prevented the reduced encapsulation efficiency under high concentrations of NaCl compared to DSPC despite the fact that it is composed of fluidic oleoyl scaffolds (Figure 4D). This can be explained by the fact that a primary amino group of DOPE is a proton donor and therefore a DOPE-containing lipid membrane is able to form direct hydrogen bonding with phosphate groups of RNA [40, 41].

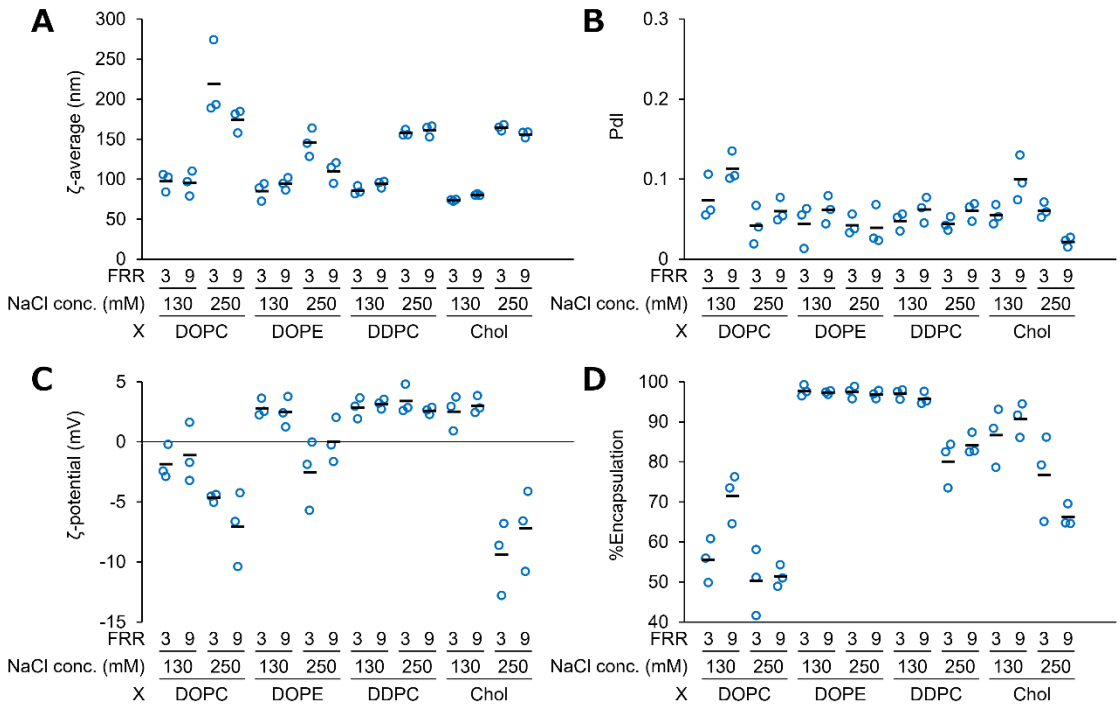

Figure 4. Physicochemical properties of the siRNA-loaded LNPs determined based on FFD. ζ-Average (A), PdI (B), ζ-potential (C), and percentage of siRNA encapsulation (D) of the LNPs. n=3.

To examine the effect of the type of CL on reactivity against NaCl, we used YSK05, a pH-sensitive cationic lipid that was previously developed in our laboratory [42]. LNPs composed of a fixed composition (YSK05/cholesterol/PEG-DMG=50/50/1, N/P ratio: 6.2) were synthesized with formulation conditions with a fixed TFR of 500 µL/min, a fixed FRR of 3, a fixed pH 4.0, and varied NaCl concentrations from 0 to 500 mM. A NaCl concentration-dependent increase in LNP size was observed, but the size was only 117 nm, even at 500 mM NaCl (Figure S13A), while CL4H6-LNPs (without PL) with even higher %PEG (1.5) reached sizes of over 150 nm at 250 mM NaCl (Figure 4A). In addition, no decrease in encapsulation efficiency (> 90%) was observed in the case of the

YSK05-LNPs even at 500 mM NaCl (Figure S13B), which was not in case for the CL4H6-LNPs without PL (Figure 4D). These results indicate that the reactivity of YSK05 with added NaCl was lower than that of CL4H6, suggesting that the fine-tuning of formulation condition is needed to produce LNPs with precisely specific properties (*e.g.* size) when a type of CL was changed.

3.4 Effect of ion species on the size of LNPs

Hofmeister effects are known to be due to the relative effect of both anions and cations and different specificities are produced on a wide range of phenomena including critical micelle concentration, ζ-potential of colloids and so on [43, 44]. In Hofmeister's original work, ions were ordered according to their ability to stabilize negatively charged proteins (hydrophobic colloids), providing the following rankings (partially described): (kosmotropic) SO_4^{2-} > Cl^- > Br^- (chaotropic) for anions, and (chaotropic) Li^+ > Na^+ > K^+ (kosmotropic) for cations [45]. In general, small or multiply charged ions with a high charge density such as Li^+ and SO_4^{2-} are well hydrated and are kosmotropes, whereas large and singly charged ions with a low charge density such as K^+ and Br^- are less hydrated and are chaotropes in the above rankings. As described above, the cationic liposome-like particles, which are initially formed after mixing with lipid components and RNAs would be hydrophobic cationic colloids. Less hydrated chaotropes preferentially interact with a hydrophobic interface due to the relatively lower interaction between a hydrophobic interface and water. Therefore, it would be expected that anionic chaotropes (*i.e.* Br^-) would preferentially interact with the cationic liposome-like particles, resulting in the efficient neutralization of the particles and in promoting particle growth (Figure 5A). Conversely, cationic kosmotrope (*i.e.* K^+) would be expected to preferentially interact with the cationic liposome-like particles, resulting in increased electrostatic repulsions between the particles thus preventing particle growth (Figure 5A). Four different salts, KCl, LiCl, Na_2SO_4, and NaBr in addition to NaCl were used to confirm the effect of ion species on the size of LNPs. Because SO_4^{2-} is a divalent ion, the molar concentration of Na^+ for Na_2SO_4 was 2-fold higher than indicated. In this study, LNPs with a fixed lipid composition (CL4H6/DOPE/cholesterol/PEG-DMG=50/10/40/1 mol%, N/P ratio: 10) were synthesized by formulation conditions with a fixed TFR (500 μL/min), a fixed FRR (3), a fixed lipid concentration (10 mM), and a varied salt concentration (130 or 250 mM) and varied salt types described above. Size as well as other physicochemical properties were measured (Figure 5B-E and S14). Significant differences in the size of LNPs were observed, especially in the case of cations. Chaotropic K^+ ion strongly prevented particle growth (< 150 nm at 250 mM) whereas kosmotropic Li^+ ion failed to prevent it (~200 nm at 250 mM) (Figure 5C). In addition, for anions, the chaotropic Br^- ion significantly promoted particle growth at 250 mM (Figure 5E). The effect of Na_2SO_4 on the size of LNPs would be expected to be higher than others in the case of only DLVO theory but not when Hofmeister effects are considered, because of both the presence of divalent anions (SO_4^{2-}) and a 2-fold higher concentration of monovalent cations (Na^+) only for Na_2SO_4. However, the actual effect

of Na_2SO_4 was consistent with NaCl and significantly lower than that for NaBr (Figure 5E). These results were in good agreement with our expectation. Interestingly, the effect of cations, which have the same positive sign as the liposome-like particles, was higher than that of anions in this case. However, the issue of whether the order of ions can be changed by hydrophilicity/hydrophobicity as well as the charge sign of the particles is not known [46]. Therefore, the impact of the ions examined in this study can be changed by the lipid composition, the pH of the system as well as related issues.

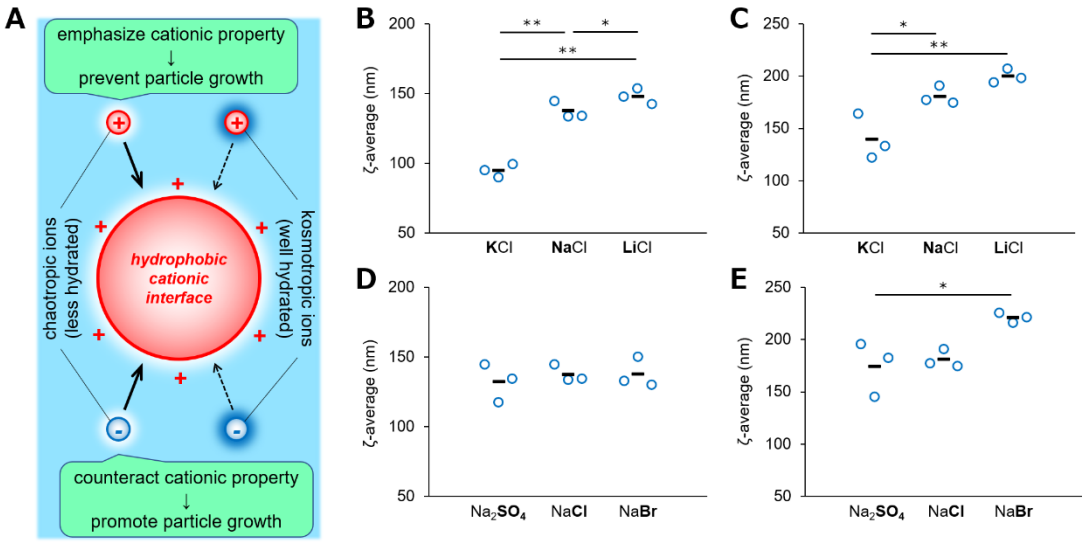

Figure 5. Effect of ion species on the size of siRNA-loaded LNPs. (A) A schematic illustration of interaction of cationic/anionic kosmotropes/chaotropes with hydrophobic cationic particles. (B-E) ζ-Average of the siRNA-loaded LNPs synthesized with 130 mM (B, D) and 250 mM (C, E) of the indicated salts. Effect of cationic (B, C) and anionic (D, E) ion species were examined. n=3. *p<0.05, **p<0.01.

3.5 Impact of NaCl addition on the delivery of mRNA to splenic DCs for cancer immunotherapy

DCs can initiate immune responses upon the early sensing of pathogens as well as cancerous tumors. Lymphoid tissues such as the spleen, where DCs are in close proximity to T cells, are preferable microenvironments for the priming and amplification of T cell responses. Therefore, delivery of cancer antigen-encoding mRNAs to splenic DCs is an attractive strategy for cancer immunotherapy. It is known that macropinocytosis, which is a unique pathway characterized by the nonspecific internalization of large amounts of extracellular fluid, is constitutively active in immature DCs [33, 47]. Therefore, an increase in the size of LNPs would be reasonable strategy for efficiently delivering payloads to DCs. We first examined the impact of LNP size on the delivery of siRNA. The siCD45-loaded DiO-labeled LNPs with a fixed lipid composition (CL4H6/DOPE/cholesterol/PEG-DMG=50/10/40/1 mol%, N/P ratio: 10) were synthesized by formulation conditions that included a

fixed TFR (500 μL/min), a fixed FRR (3), a fixed lipid concentration (16 mM), and varied salt concentrations (10 or 370 mM) (coded as D1 and D2) (Table 4). Twenty-four hours after an intravenous injection of the LNPs, cellular uptake in splenic DCs was measured by flowcytometry. Splenic DCs were sorted, and CD45 gene expression was measured by quantitative RT-PCR. The cellular uptake of the D2-LNP preparation was approximately 10-fold higher than that for the D1-LNPs (Figure 6A). Reflected by the enhanced cellular uptake, the gene silencing activity of the D2-LNPs (~59%) were significantly higher than that for the D1-LNPs (~26%) (Figure 6B). Next, the mNluc-loaded LNPs with a fixed lipid composition (CL4H6/DOPE/cholesterol/PEG-DMG=50/10/40/1 mol%, N/P ratio: 10) were synthesized by formulation conditions with a fixed TFR (500 μL/min), a fixed FRR (3), a fixed lipid concentration. (16 mM), and varied salt concentrations. (10, 250 or 370 mM) (coded as E1 to E3) (Table 5). The mNluc-LNPs were uniform, became larger depending on the concentration of NaCl used up to a size of approximately 200 nm, and showed a gradual decrease in encapsulation efficiency to 76%, which was essentially consistent with the results in siRNA-loaded LNPs. The mNluc-loaded LNPs with different sizes were intravenously injected to mice and the Nluc activity in the sorted 3,000 splenic DCs was then measured. As expected, the largest E3-LNPs showed a significantly higher Nluc expression compared with the smaller counterparts (Figure 6C). The mNluc used in this study, which is chemically unmodified IVT mRNA, would stimulate an innate immune response upon being detected by a microbial-associated molecular pattern surveillance system including the endosomal toll-like receptor (TLR) 7/8 [48]. In addition, potential contamination of double-stranded RNAs in IVT mRNA can be detected by endosomal TLR3 and the cytosolic RNA sensors retinoic acid–inducible gene I and melanoma differentiation-associated protein 5, and also activate innate immune response [49, 50]. Therefore, the mRNA used in this study would be immunogenic and activate DCs and other lymphocytes. As expected, the E3-LNPs induced a higher I-A/I-E (a maturation marker) expression in splenic DCs compared to smaller counterparts (Figure 6D). Several activation markers in splenic DCs and lymphocytes were then measured after a single injection of E1- or E3-LNPs. The expression of all activation markers in splenic DCs including CD40, CD80, and CD86 was significantly higher for the larger E3-LNPs (Figure 6E-6I). Similarly, both $CD3^+$ T cells and $CD19^+$ B cells were also strongly activated be the E3-LNPs (Figure 6H, 6I). These data suggest that larger E3-LNPs can deliver mRNA, induce transgene expression and maturation of splenic DCs, and activate lymphocytes as well more efficiently than smaller counterparts. Motivated by these findings, the immunotherapeutic effect of the E3-LNPs was investigated in an E.G7-OVA-bearing mouse model. The mOVA-loaded E1- or E3-LNPs were intravenously injected to tumor-bearing mice at 7 and 10 days after tumor inoculation and tumor size was measured for up to day 18 (Figure 6J). The E1-LNPs significantly reduced tumor growth but failed to shrink tumor tissues (Figure 6K). On the other hand, the shrinking of tumor tissues was clearly observed in all mice that had been given the E3-LNPs from day 14. Taken together, biological effect of the RNA-loaded LNPs could be changed

significantly by controlling size of the LNPs through modification of formulation conditions, including the concentration of salt used in their preparation. These findings suggest that optimization of formulation conditions including salt concentration is as important as in the optimization of a formulation itself for maximizing biological effect of RNA-loaded LNPs.

Table 4. Physicochemical properties of the siCD45-loaded LNPs with constant lipid compositions (D1 and D2) synthesized using different NaCl concentrations.

Entry	NaCl conc. (mM)	ζ-average (nm)	Number mean (nm)	PdI	ζ-potential (mV)	%Encapsulation
D1	10	116	63	0.22	3.4	96.5
D2	370	270	245	0.03	0.1	98.9

Table 5. Physicochemical properties of the mRNA-loaded LNPs with constant lipid compositions (E1 to E3) synthesized using different NaCl concentrations.

Entry	NaCl conc. (mM)	ζ-average (nm)	Number mean (nm)	PdI	ζ-potential (mV)	%Encapsulation
E1	10	91±14	45±7	0.27±0.06	1.4±0.1	90.6±1.8
E2	250	137±39	98±32	0.11±0.01	1.5±1.2	84.2±4.8
E3	370	195±32	154±42	0.10±0.03	0.7±0.4	76.0±5.9

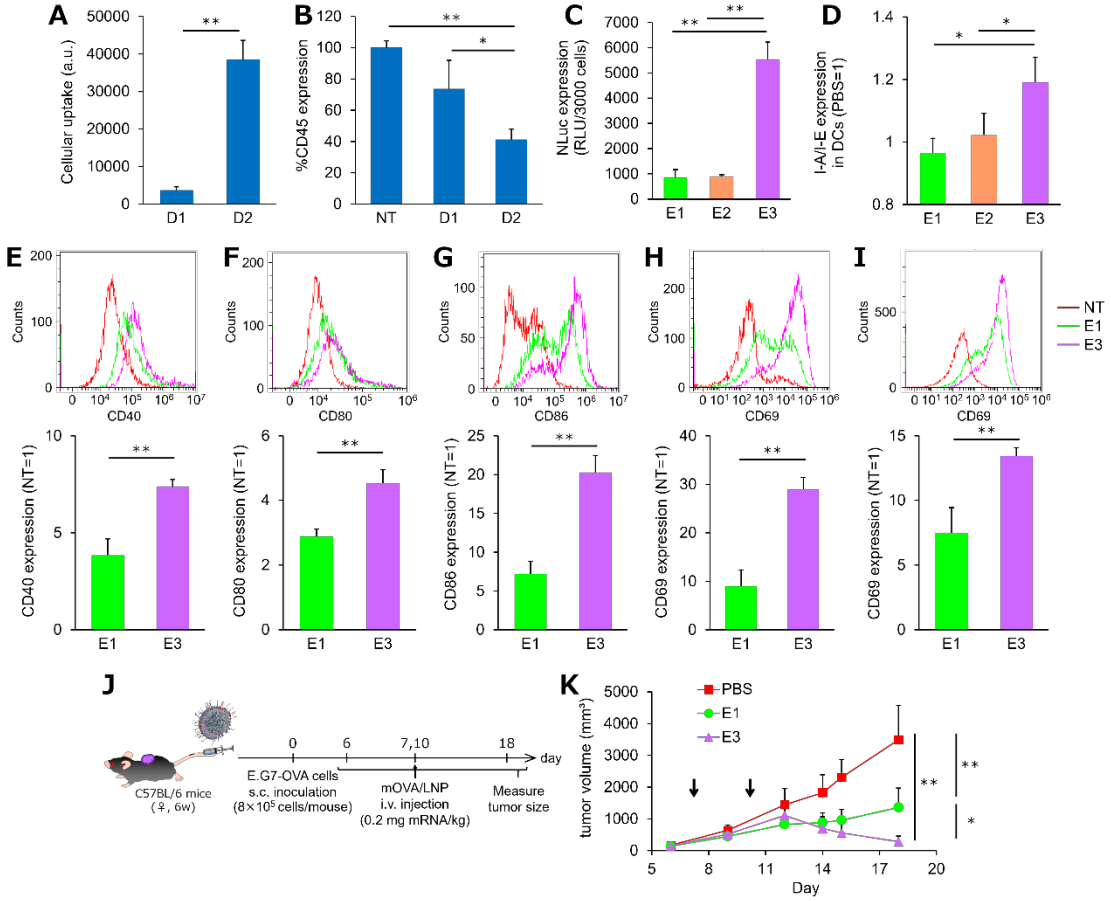

Figure 6. Effect of the size of siRNA or mRNA-loaded LNPs on *in vivo* delivery of siRNA or mRNA and biological effects. (A) Cellular uptake of the siCD45-loaded LNPs in splenic DCs. n=3. (B) CD45 gene expression in the sorted splenic DCs. n=3. (C) Nluc transgene expression in the sorted splenic DCs. n=3-4. (D) Relative I-A/I-E expression levels in splenic DCs. n=3-4. (E-I) Relative expression levels of activation markers in splenic DCs and lymphocytes. Relative expression levels of CD40 (E), CD80 (F), and CD86 (G) in splenic DCs, and CD69 in splenic T cells (H) and B cells (I) were measured. n=3. (J, K) Therapeutic effect of the mOVA-loaded LNPs on tumor-bearing mouse model. Time course (J) and therapeutic antitumor effect of the LNPs (K). n=5. **p*<0.05, ***p*<0.01.

4. Conclusions

In the present study, several formulation conditions for preparing RNA-loaded LNPs using a microfluidic device were systematically examined by DOE. The effect of the formulation conditions was in good agreement with our hypothesis based on DLVO theory. Salt concentration was the most significant factor for the size of LNPs and contributed to the formation of larger LNPs (> 200 nm) than reported. The effect of salt on the size of LNPs followed Hofmeister's effects. Specifically, both chaotropic cations and anions contributed to the formation of larger LNPs compared to kosmotropes because the initially formed liposome-like particles are hydrophobic and cationic. Increasing the size of the mRNA-loaded LNPs resulted in improved transgene expression and the maturation of splenic DCs, in stronger activation of lymphocytes, and in a better therapeutic effect in an E.G7-OVA-bearing mouse model. These findings suggest that optimization of the formulation conditions is as important in terms of maximizing the biological effect of RNA-loaded LNPs, and the formulation parameters examined in this study, including the concentration of and the type of salt used, contribute to developing more potent LNPs.

Acknowledgements

This work was supported, in part, by JST, PRESTO Grant Number JPMJPR19K8, Japan, Hokkaido University Support Program for Frontier Research, The Mochida Memorial Foundation for Medical and Pharmaceutical Research, and the Special Education and Research Expenses from the Ministry of Education, Culture, Sports, Science and Technology. The authors also wish to thank Dr. Milton S. Feather for his helpful advice in preparing the English manuscript.

Conflict of interest

The authors who have taken part in this study declare that they have nothing to disclose regarding funding or conflict of interest with respect to this manuscript.

References

[1] U. Sahin, K. Karikó, Ö. Türeci, mRNA-based therapeutics--developing a new class of drugs, Nat Rev Drug Discov, 13 (2014) 759-780.

[2] R. Rupaimoole, F.J. Slack, MicroRNA therapeutics: towards a new era for the management of cancer and other diseases, Nat Rev Drug Discov, 16 (2017) 203-222.

[3] K. Paunovska, D. Loughrey, J.E. Dahlman, Drug delivery systems for RNA therapeutics, Nature reviews. Genetics, (2022) 1-16.

[4] M.D. Buschmann, M.J. Carrasco, S. Alishetty, M. Paige, M.G. Alameh, D. Weissman, Nanomaterial Delivery Systems for mRNA Vaccines, Vaccines (Basel), 9 (2021).

[5] S.M. Hoy, Patisiran: First Global Approval, Drugs, 78 (2018) 1625-1631.

[6] Y.N. Lamb, BNT162b2 mRNA COVID-19 Vaccine: First Approval, Drugs, 81 (2021) 495-501.

[7] Y. Sato, Development of Lipid Nanoparticles for the Delivery of Macromolecules Based on the Molecular Design of pH-Sensitive Cationic Lipids, Chem Pharm Bull (Tokyo), 69 (2021) 1141-1159.

[8] Y. Sato, Y. Kinami, K. Hashiba, H. Harashima, Different kinetics for the hepatic uptake of lipid nanoparticles between the apolipoprotein E/low density lipoprotein receptor and the N-acetyl-d-galactosamine/asialoglycoprotein receptor pathway, J Control Release, 322 (2020) 217-226.

[9] A. Akinc, W. Querbes, S. De, J. Qin, M. Frank-Kamenetsky, K.N. Jayaprakash, M. Jayaraman, K.G. Rajeev, W.L. Cantley, J.R. Dorkin, J.S. Butler, L. Qin, T. Racie, A. Sprague, E. Fava, A. Zeigerer, M.J. Hope, M. Zerial, D.W. Sah, K. Fitzgerald, M.A. Tracy, M. Manoharan, V. Koteliansky, A. Fougerolles, M.A. Maier, Targeted delivery of RNAi therapeutics with endogenous and exogenous ligand-based mechanisms, Mol Ther, 18 (2010) 1357-1364.

[10] S. Rietwyk, D. Peer, Next-Generation Lipids in RNA Interference Therapeutics, ACS Nano, 11 (2017) 7572-7586.

[11] S.C. Semple, A. Akinc, J. Chen, A.P. Sandhu, B.L. Mui, C.K. Cho, D.W. Sah, D. Stebbing, E.J. Crosley, E. Yaworski, I.M. Hafez, J.R. Dorkin, J. Qin, K. Lam, K.G. Rajeev, K.F. Wong, L.B. Jeffs, L. Nechev, M.L. Eisenhardt, M. Jayaraman, M. Kazem, M.A. Maier, M. Srinivasulu, M.J. Weinstein, Q. Chen, R. Alvarez, S.A. Barros, S. De, S.K. Klimuk, T. Borland, V. Kosovrasti, W.L. Cantley, Y.K. Tam, M. Manoharan, M.A. Ciufolini, M.A. Tracy, A. de Fougerolles, I. MacLachlan, P.R. Cullis, T.D. Madden, M.J. Hope, Rational design of cationic lipids for siRNA delivery, Nat Biotechnol, 28 (2010) 172-176.

[12] T.S. Zimmermann, A.C. Lee, A. Akinc, B. Bramlage, D. Bumcrot, M.N. Fedoruk, J. Harborth, J.A. Heyes, L.B. Jeffs, M. John, A.D. Judge, K. Lam, K. McClintock, L.V. Nechev, L.R. Palmer, T. Racie, I. Röhl, S. Seiffert, S. Shanmugam, V. Sood, J. Soutschek, I. Toudjarska, A.J. Wheat, E. Yaworski, W. Zedalis, V. Koteliansky, M. Manoharan, H.P. Vornlocher, I. MacLachlan, RNAi-

mediated gene silencing in non-human primates, Nature, 441 (2006) 111-114.
[13] Y. Sato, K. Hashiba, K. Sasaki, M. Maeki, M. Tokeshi, H. Harashima, Understanding structure-activity relationships of pH-sensitive cationic lipids facilitates the rational identification of promising lipid nanoparticles for delivering siRNAs in vivo, J Control Release, 295 (2019) 140-152.
[14] M.A. Maier, M. Jayaraman, S. Matsuda, J. Liu, S. Barros, W. Querbes, Y.K. Tam, S.M. Ansell, V. Kumar, J. Qin, X. Zhang, Q. Wang, S. Panesar, R. Hutabarat, M. Carioto, J. Hettinger, P. Kandasamy, D. Butler, K.G. Rajeev, B. Pang, K. Charisse, K. Fitzgerald, B.L. Mui, X. Du, P. Cullis, T.D. Madden, M.J. Hope, M. Manoharan, A. Akinc, Biodegradable lipids enabling rapidly eliminated lipid nanoparticles for systemic delivery of RNAi therapeutics, Mol Ther, 21 (2013) 1570-1578.
[15] M. Jayaraman, S.M. Ansell, B.L. Mui, Y.K. Tam, J. Chen, X. Du, D. Butler, L. Eltepu, S. Matsuda, J.K. Narayanannair, K.G. Rajeev, I.M. Hafez, A. Akinc, M.A. Maier, M.A. Tracy, P.R. Cullis, T.D. Madden, M. Manoharan, M.J. Hope, Maximizing the potency of siRNA lipid nanoparticles for hepatic gene silencing in vivo, Angew Chem Int Ed Engl, 51 (2012) 8529-8533.
[16] S.J. Shepherd, D. Issadore, M.J. Mitchell, Microfluidic formulation of nanoparticles for biomedical applications, Biomaterials, 274 (2021) 120826.
[17] I.V. Zhigaltsev, N. Belliveau, I. Hafez, A.K. Leung, J. Huft, C. Hansen, P.R. Cullis, Bottom-up design and synthesis of limit size lipid nanoparticle systems with aqueous and triglyceride cores using millisecond microfluidic mixing, Langmuir, 28 (2012) 3633-3640.
[18] N. Kimura, M. Maeki, Y. Sato, Y. Note, A. Ishida, H. Tani, H. Harashima, M. Tokeshi, Development of the iLiNP Device: Fine Tuning the Lipid Nanoparticle Size within 10 nm for Drug Delivery, Acs Omega, 3 (2018) 5044-5051.
[19] J.A. Kulkarni, M.M. Darjuan, J.E. Mercer, S. Chen, R. van der Meel, J.L. Thewalt, Y.Y.C. Tam, P.R. Cullis, On the Formation and Morphology of Lipid Nanoparticles Containing Ionizable Cationic Lipids and siRNA, ACS Nano, 12 (2018) 4787-4795.
[20] J.A. Kulkarni, D. Witzigmann, J. Leung, R. van der Meel, J. Zaifman, M.M. Darjuan, H.M. Grisch-Chan, B. Thöny, Y.Y.C. Tam, P.R. Cullis, Fusion-dependent formation of lipid nanoparticles containing macromolecular payloads, Nanoscale, 11 (2019) 9023-9031.
[21] M. Yanez Arteta, T. Kjellman, S. Bartesaghi, S. Wallin, X. Wu, A.J. Kvist, A. Dabkowska, N. Székely, A. Radulescu, J. Bergenholtz, L. Lindfors, Successful reprogramming of cellular protein production through mRNA delivered by functionalized lipid nanoparticles, Proc Natl Acad Sci U S A, 115 (2018) E3351-E3360.
[22] N.M. Belliveau, J. Huft, P.J. Lin, S. Chen, A.K. Leung, T.J. Leaver, A.W. Wild, J.B. Lee, R.J. Taylor, Y.K. Tam, C.L. Hansen, P.R. Cullis, Microfluidic Synthesis of Highly Potent Limit-size Lipid Nanoparticles for In Vivo Delivery of siRNA, Mol Ther Nucleic Acids, 1 (2012) e37.

[23] Y. Sato, Y. Note, M. Maeki, N. Kaji, Y. Baba, M. Tokeshi, H. Harashima, Elucidation of the physicochemical properties and potency of siRNA-loaded small-sized lipid nanoparticles for siRNA delivery, J Control Release, 229 (2016) 48-57.
[24] Y. Sato, N. Okabe, Y. Note, K. Hashiba, M. Maeki, M. Tokeshi, H. Harashima, Hydrophobic scaffolds of pH-sensitive cationic lipids contribute to miscibility with phospholipids and improve the efficiency of delivering short interfering RNA by small-sized lipid nanoparticles, Acta Biomater, 102 (2020) 341-350.
[25] S. Rex, M.J. Zuckermann, M. Lafleur, J.R. Silvius, Experimental and Monte Carlo simulation studies of the thermodynamics of polyethyleneglycol chains grafted to lipid bilayers, Biophys J, 75 (1998) 2900-2914.
[26] M. Alwarawrah, J. Dai, J. Huang, A molecular view of the cholesterol condensing effect in DOPC lipid bilayers, J Phys Chem B, 114 (2010) 7516-7523.
[27] C.B. Roces, G. Lou, N. Jain, S. Abraham, A. Thomas, G.W. Halbert, Y. Perrie, Manufacturing Considerations for the Development of Lipid Nanoparticles Using Microfluidics, Pharmaceutics, 12 (2020).
[28] T. Terada, J.A. Kulkarni, A. Huynh, S. Chen, R. van der Meel, Y.Y.C. Tam, P.R. Cullis, Characterization of Lipid Nanoparticles Containing Ionizable Cationic Lipids Using Design-of-Experiments Approach, Langmuir, 37 (2021) 1120-1128.
[29] K.J. Hassett, J. Higgins, A. Woods, B. Levy, Y. Xia, C.J. Hsiao, E. Acosta, Ö. Almarsson, M.J. Moore, L.A. Brito, Impact of lipid nanoparticle size on mRNA vaccine immunogenicity, J Control Release, 335 (2021) 237-246.
[30] E. Kastner, R. Kaur, D. Lowry, B. Moghaddam, A. Wilkinson, Y. Perrie, High-throughput manufacturing of size-tuned liposomes by a new microfluidics method using enhanced statistical tools for characterization, Int J Pharm, 477 (2014) 361-368.
[31] Y. Sato, H. Hatakeyama, M. Hyodo, H. Harashima, Relationship Between the Physicochemical Properties of Lipid Nanoparticles and the Quality of siRNA Delivery to Liver Cells, Mol Ther, 24 (2016) 788-795.
[32] F. Jacobs, E. Wisse, B. De Geest, The role of liver sinusoidal cells in hepatocyte-directed gene transfer, Am J Pathol, 176 (2010) 14-21.
[33] M. Diken, S. Kreiter, A. Selmi, C.M. Britten, C. Huber, Ö. Türeci, U. Sahin, Selective uptake of naked vaccine RNA by dendritic cells is driven by macropinocytosis and abrogated upon DC maturation, Gene Ther, 18 (2011) 702-708.
[34] X.P. Lin, J.D. Mintern, P.A. Gleeson, Macropinocytosis in Different Cell Types: Similarities and Differences, Membranes (Basel), 10 (2020).
[35] J. Zhang, Y. Pei, H. Zhang, L. Wang, L. Arrington, Y. Zhang, A. Glass, A.M. Leone, Assessing the heterogeneity level in lipid nanoparticles for siRNA delivery: size-based separation,

compositional heterogeneity, and impact on bioperformance, Mol Pharm, 10 (2013) 397-405.
[36] N.A. Mishchuk, The model of hydrophobic attraction in the framework of classical DLVO forces, Adv Colloid Interface Sci, 168 (2011) 149-166.
[37] A. Hashiba, M. Toyooka, Y. Sato, M. Maeki, M. Tokeshi, H. Harashima, The use of design of experiments with multiple responses to determine optimal formulations for in vivo hepatic mRNA delivery, J Control Release, 327 (2020) 467-476.
[38] N.T.K. Thanh, N. Maclean, S. Mahiddine, Mechanisms of Nucleation and Growth of Nanoparticles in Solution, Chemical reviews, 114 (2014) 7610-7630.
[39] E. Wisse, F. Jacobs, B. Topal, P. Frederik, B. De Geest, The size of endothelial fenestrae in human liver sinusoids: implications for hepatocyte-directed gene transfer, Gene Ther, 15 (2008) 1193-1199.
[40] Y. Suzuki, H. Onuma, R. Sato, Y. Sato, A. Hashiba, M. Maeki, M. Tokeshi, M.E.H. Kayesh, M. Kohara, K. Tsukiyama-Kohara, H. Harashima, Lipid nanoparticles loaded with ribonucleoprotein-oligonucleotide complexes synthesized using a microfluidic device exhibit robust genome editing and hepatitis B virus inhibition, J Control Release, 330 (2021) 61-71.
[41] H. Hong, Toward understanding driving forces in membrane protein folding, Arch Biochem Biophys, 564 (2014) 297-313.
[42] Y. Sato, H. Hatakeyama, Y. Sakurai, M. Hyodo, H. Akita, H. Harashima, A pH-sensitive cationic lipid facilitates the delivery of liposomal siRNA and gene silencing activity in vitro and in vivo, J Control Release, 163 (2012) 267-276.
[43] B.L. Bales, A Definition of the Degree of Ionization of a Micelle Based on Its Aggregation Number, The Journal of Physical Chemistry B, 105 (2001) 6798-6804.
[44] T. López-León, A.B. Jódar-Reyes, D. Bastos-González, J.L. Ortega-Vinuesa, Hofmeister Effects in the Stability and Electrophoretic Mobility of Polystyrene Latex Particles, The Journal of Physical Chemistry B, 107 (2003) 5696-5708.
[45] W. Kunz, J. Henle, B.W. Ninham, 'Zur Lehre von der Wirkung der Salze' (about the science of the effect of salts): Franz Hofmeister's historical papers, Current Opinion in Colloid & Interface Science, 9 (2004) 19-37.
[46] T. López-León, M.J. Santander-Ortega, J.L. Ortega-Vinuesa, D. Bastos-González, Hofmeister Effects in Colloidal Systems: Influence of the Surface Nature, The Journal of Physical Chemistry C, 112 (2008) 16060-16069.
[47] L.M. Kranz, M. Diken, H. Haas, S. Kreiter, C. Loquai, K.C. Reuter, M. Meng, D. Fritz, F. Vascotto, H. Hefesha, C. Grunwitz, M. Vormehr, Y. Hüsemann, A. Selmi, A.N. Kuhn, J. Buck, E. Derhovanessian, R. Rae, S. Attig, J. Diekmann, R.A. Jabulowsky, S. Heesch, J. Hassel, P. Langguth, S. Grabbe, C. Huber, Ö. Türeci, U. Sahin, Systemic RNA delivery to dendritic cells exploits antiviral defence for cancer immunotherapy, Nature, 534 (2016) 396-401.

[48] F. Heil, H. Hemmi, H. Hochrein, F. Ampenberger, C. Kirschning, S. Akira, G. Lipford, H. Wagner, S. Bauer, Species-specific recognition of single-stranded RNA via toll-like receptor 7 and 8, Science, 303 (2004) 1526-1529.
[49] N. Dauletbaev, M. Cammisano, K. Herscovitch, L.C. Lands, Stimulation of the RIG-I/MAVS Pathway by Polyinosinic:Polycytidylic Acid Upregulates IFN-β in Airway Epithelial Cells with Minimal Costimulation of IL-8, J Immunol, 195 (2015) 2829-2841.
[50] J. Nelson, E.W. Sorensen, S. Mintri, A.E. Rabideau, W. Zheng, G. Besin, N. Khatwani, S.V. Su, E.J. Miracco, W.J. Issa, S. Hoge, M.G. Stanton, J.L. Joyal, Impact of mRNA chemistry and manufacturing process on innate immune activation, Sci Adv, 6 (2020) eaaz6893.

Figure captions

Figure 1. Physicochemical properties of RNA-loaded LNPs are related to formulation parameters. (A) Schematic illustration of synthesis of RNA-loaded LNPs using microfluidic device, formulation parameters and physicochemical properties of the LNPs examined in this study. (B) Formula representing DLVO theory.

Figure 2. Physicochemical properties of the siRNA-loaded LNPs (A1 to A17). (A-D) ζ-Average (A), PdI (B), ζ-potential (C), and percentage of siRNA encapsulation (D) of the LNPs. n=3. (E) A regression equation for the size of siRNA-loaded LNPs determined by the DOE. (F) Plasma FVII protein levels after intravenous injection of siFVII-loaded B1- to B5-LNPs. n=3-8. *p<0.05, **p<0.01.

Figure 3. Physicochemical properties of the siRNA-loaded LNPs (C1 to C27).ζ-Average (A), PdI (B), ζ-potential (C), and percentage of siRNA encapsulation (D) of the LNPs. n=3.

Figure 4. Physicochemical properties of the siRNA-loaded LNPs determined based on FFD. ζ-Average (A), PdI (B), ζ-potential (C), and percentage of siRNA encapsulation (D) of the LNPs. n=3.

Figure 5. Effect of ion species on the size of siRNA-loaded LNPs. (A) A schematic illustration of interaction of cationic/anionic kosmotropes/chaotropes with hydrophobic cationic particles. (B-E) ζ-Average of the siRNA-loaded LNPs synthesized with 130 mM (B, D) and 250 mM (C, E) of the indicated salts. Effect of cationic (B, C) and anionic (D, E) ion species were examined. n=3. *p<0.05, **p<0.01.

Figure 6. Effect of the size of siRNA or mRNA-loaded LNPs on *in vivo* delivery of siRNA or mRNA and biological effects. (A) Cellular uptake of siCD45-loaded LNPs in splenic DCs. n=3. (B) CD45 gene expression in the sorted splenic DCs. n=3. (C) Nluc transgene expression in the sorted splenic DCs. n=3-4. (D) Relative I-A/I-E expression levels in splenic DCs. n=3-4. (E-I) Relative expression levels of activation markers in splenic DCs and lymphocytes. Relative expression levels of CD40 (E), CD80 (F), and CD86 (G) in splenic DCs, and CD69 in splenic T cells (H) and B cells (I) were measured. n=3. (J, K) Therapeutic effect of the mOVA-loaded LNPs on tumor-bearing mouse model. Time course (J) and therapeutic antitumor effect of the LNPs (K). n=5. *p<0.05, **p<0.01.

SUPPORTING INFORMATION

On the size-regulation of RNA-loaded lipid nanoparticles synthesized by microfluidic device

Kento Okuda[1] †, Yusuke Sato[1] †*, Kazuki Iwakawa[1], Kosuke Sasaki[1], Nana Okabe[1], Masatoshi Maeki[2,3], Manabu Tokeshi[2,4,5], Hideyoshi Harashima[1]**

[1]Laboratory for Molecular Design of Pharmaceutics, Faculty of Pharmaceutical Sciences, Hokkaido University, Kita-12, Nishi-6, Kita-Ku, Sapporo 060-0812, Japan.

[2]Division of Applied Chemistry, Faculty of Engineering, Hokkaido University, Kita-13, Nishi-8, Kita-Ku, Sapporo 060-8628, Japan.

[3]JST PRESTO, 4-1-8 Honcho, Kawaguchi, Saitama, 332-0012, Japan

[4]Innovative Research Center for Preventive Medical Engineering, Nagoya University, Furo-cho, Chikusa-ku, Nagoya 464-8601, Japan

[5]Institute of Nano-Life Systems, Institutes of Innovation for Future Society, Nagoya University, Furo-cho, Chikusa-ku, Nagoya 464-8601, Japan

† These authors contributed equally to this work.

**Corresponding authors:*
Yusuke Sato E-maol address: y_sato@pharm.hokudai.ac.jp Tel: +81 11 706 3734 Fax: +81 11 706 3734
Hideyoshi Harashima E-mail address: harasima@pharm.hokudai.ac.jp Tel: +81 11 706 3919 Fax: +81 11 706 4879

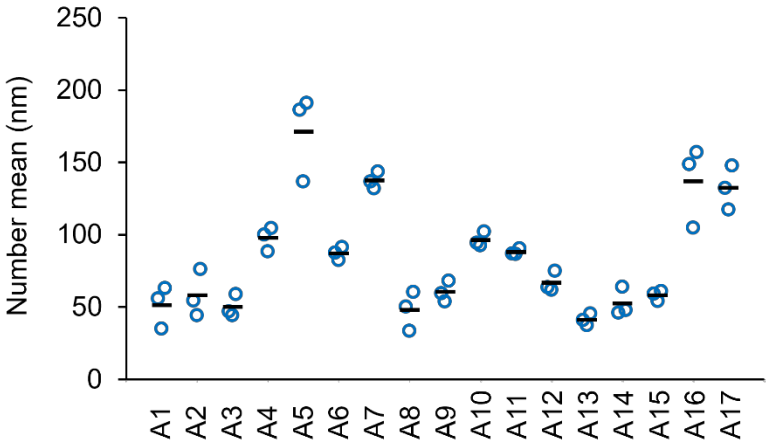

Figure S1. Number-weighted mean diameter of siRNA-loaded LNPs (related to Figure 2).

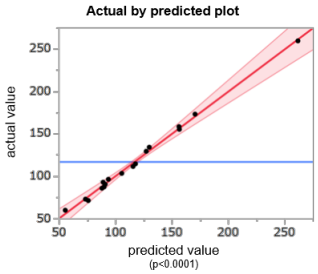

Summary of Fit	
R^2	0.996
Adjusted R^2	0.990
Root Mean Square Error	4.950
Mean	117.4
n	17

ANOVA Results			
Source	Degrees of Freedom	Sum of Squares	Mean Square
Model	10	38303.556	3830.36
Error	6	147.002	24.50
Total	16	38450.558	
F-Test Results			
	F Ratio	Prob > F	
ANOVA	156.3392	< 0.0001	

Parameter Estimates				
Term in Model	Estimate	Std. Error	t Ratio	Prob > |t|
Intercept	90.727778	2.857755	31.75	< 0.0001
TFR(100,500)	-16.38929	1.322883	-12.39	< 0.0001
FRR(3,9)	-10.00238	1.322883	-7.56	0.0003
NaCl conc.(10,250)	32.735	1.322883	24.75	< 0.0001
%PEG(1,2)	-19.23643	1.322883	-14.54	< 0.0001
Lipid conc.(4,16)	12.372619	1.322883	9.35	< 0.0001
pH(4,6)	12.416429	1.322883	9.39	< 0.0001
TFR*FRR	13.873095	1.479029	9.38	< 0.0001
FRR*NaCl conc.	-13.7569	1.479029	-9.30	< 0.0001
FRR*pH	-7.774524	1.479029	-5.26	0.0019
FRR*FRR	32.348413	3.149092	10.27	< 0.0001

Effect Tests			
Effect	Sum of Squares	F Ratio	Prob > F
TFR(100,500)	3760.522	153.4889	< 0.0001
FRR(3,9)	1400.667	57.1694	0.0003
NaCl conc.(10,250)	15002.123	612.3244	< 0.0001
%PEG(1,2)	5180.563	211.4491	< 0.0001
Lipid conc.(4,16)	2143.144	87.4742	< 0.0001
pH(4,6)	2158.348	88.0948	< 0.0001
TFR*FRR	2155.583	87.9820	< 0.0001
FRR*NaCl conc.	2119.627	86.5144	< 0.0001
FRR*pH	676.964	27.6309	0.019
FRR*FRR	2585.272	105.5201	< 0.0001

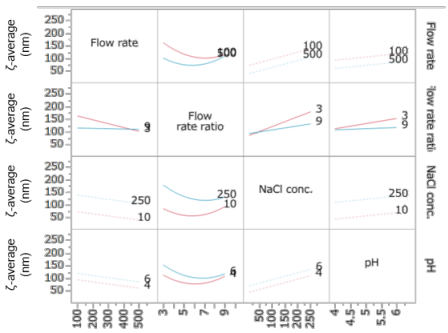

Figure S2. Statistical information regarding the effective design-based model selection for definitive screening design to predict the ζ-average of the siRNA-loaded LNPs (A1 to A17).

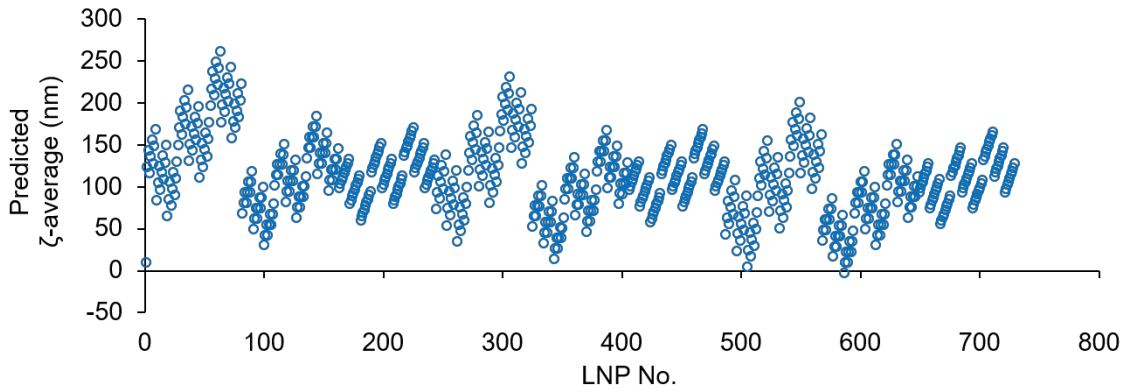

Figure S3. Predicted ζ-average of siRNA-loaded LNPs synthesized with all (723) conbinations of the formulation parameter levels using the equation shown in Figure 2E.

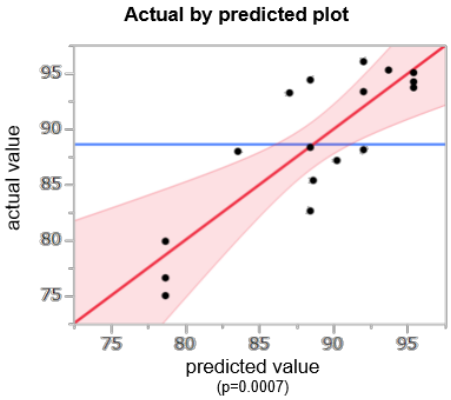

Summary of Fit	
R^2	0.717
Adjusted R^2	0.652
Root Mean Square Error	4.00
Mean	88.63
n	17

ANOVA Results			
Source	Degrees of Freedom	Sum of Squares	Mean Square
Model	3	526.38859	175.463
Error	13	207.54670	15.965
Total	16	733.93530	
F-Test Results			
	F Ratio	Prob > F	
ANOVA	10.9904	0.0007	

Parameter Estimates				
Term in Model	Estimate	Std. Error	t Ratio	Prob > |t|
Intercept	88.625985	0.969085	91.45	< 0.0001
NaCl conc.(10,250)	-5.079301	1.067879	-4.76	0.0004
Lipid conc.(4,16)	-1.596528	1.067879	-1.50	0.1588
NaCl conc.*Lipid conc.	-3.285241	1.153442	-2.85	0.0137

Effect Tests			
Effect	Sum of Squares	F Ratio	Prob > F
NaCl conc.(10,250)	361.19025	22.6237	0.0004
Lipid conc.(4,16)	35.68463	2.2352	0.1588
NaCl conc.*Lipid conc.	129.51371	8.1123	0.0137

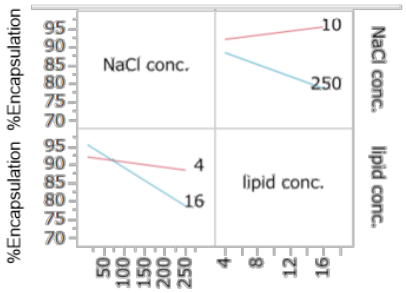

Figure S4. Statistical information regarding the effective design-based model selection for definitive screening design for predicting the percentage of siRNA encapsulation of the siRNA-loaded LNPs (A1 to A17).

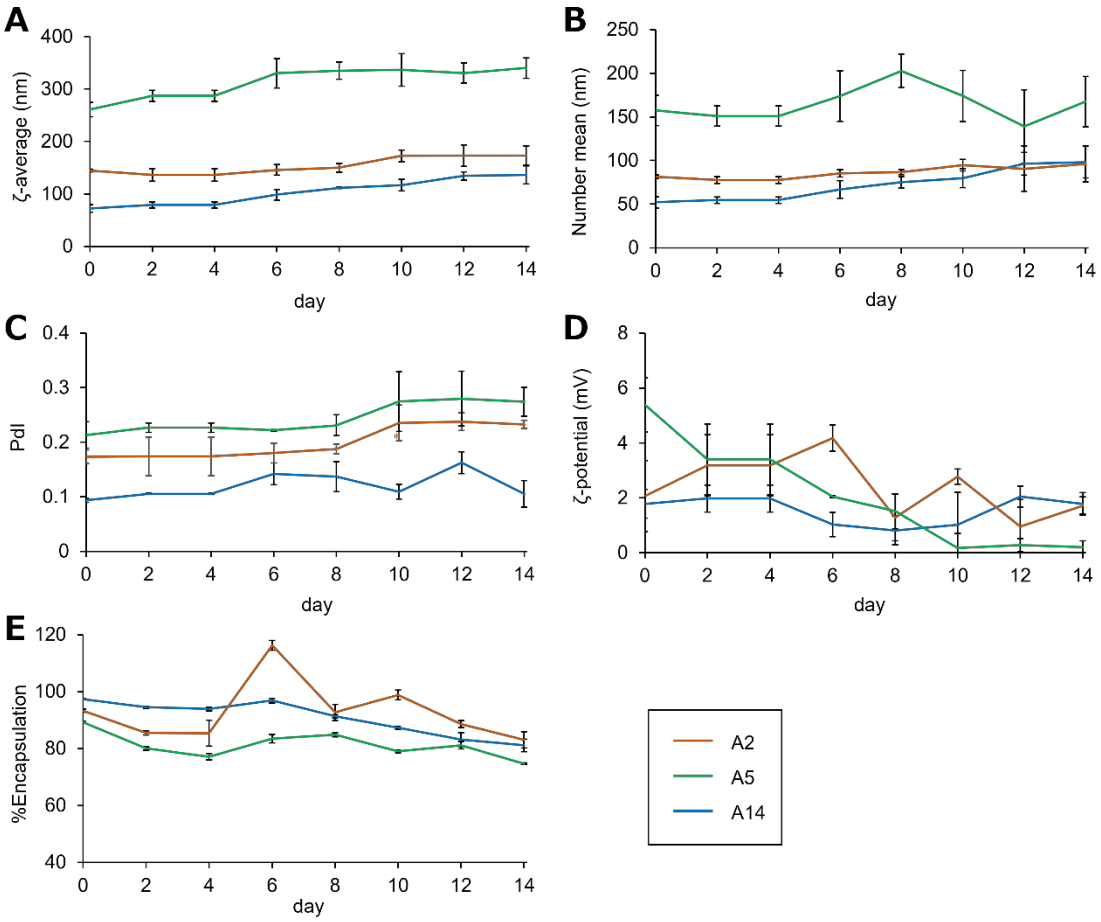

Figure S5. Evaluation of the stability of the siRNA-loaded LNPs. Three LNPs synthesized using different conditions were stored at 4°C as a wet preparation for up to 2 weeks. ζ-Average (A), Number mean (B), PdI (C), ζ-potential (D), and percentage of siRNA encapsulation (E) of the LNPs were measured after storage for the indicated time. n=3.

A

NaCl (mM)	ζ-average (nm)	Number mean (nm)	PdI	ζ-potential (mV)	%Encapsulation
10	76	57	0.55	3.9	96.8
130	91	70	0.1	5.2	97
250	147	116	0.08	5.5	96.7
370	229	208	0.02	5.8	95.4

B

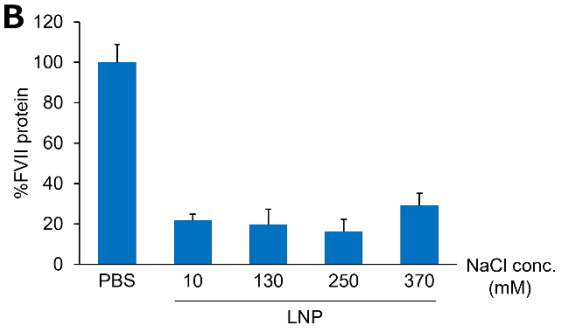

Figure S6. Physicochemical properties and FVII gene silencing activity of the siFVII-loaded LNPs prepared under different NaCl concentrations from 10 to 370 mM. (A) Physicochemical properties. (B) FVII gene silencing activity. n=3.

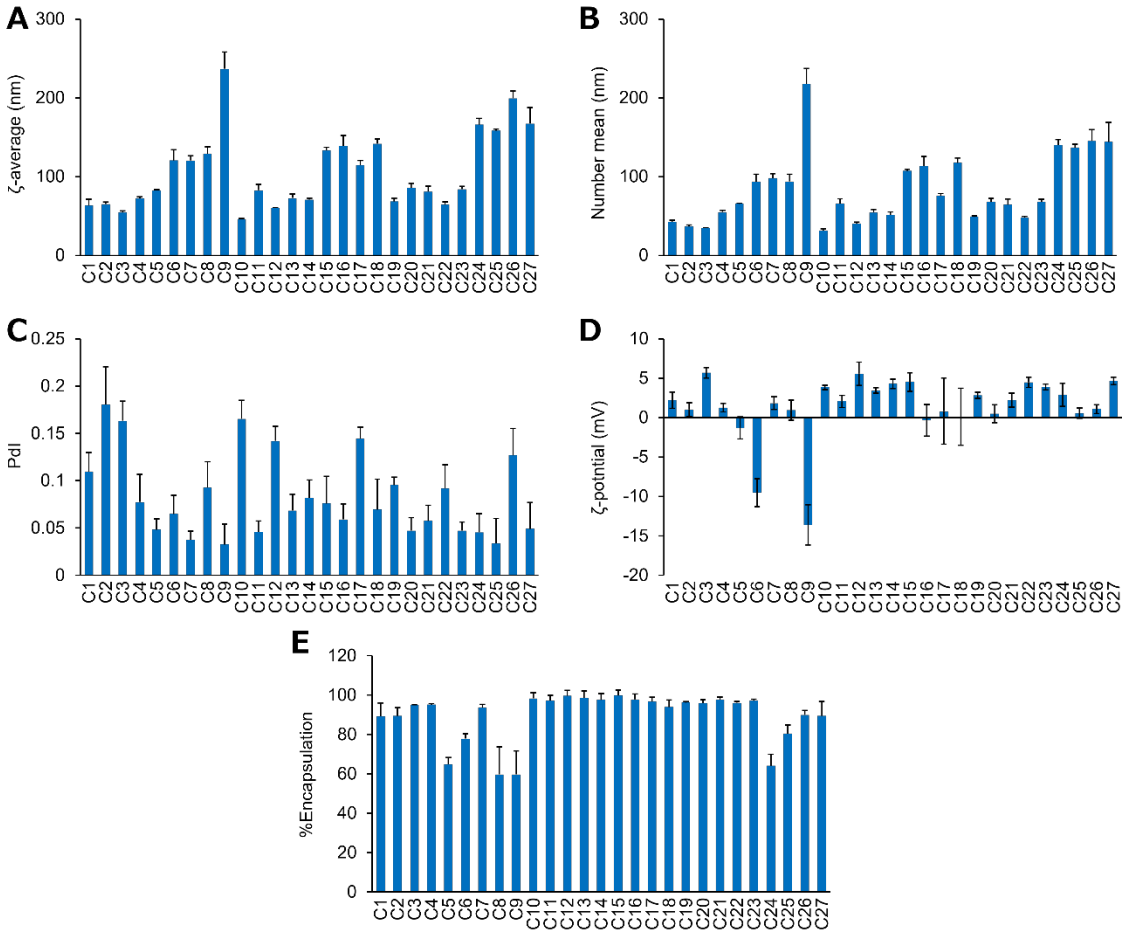

Figure S7. Physicochemical properties of the siRNA-loaded LNPs (C1 to C27). (A-E) ζ-Average (A), number mean (B), PdI (C), ζ-potential (D), and percentage of siRNA encapsulation (E) of the LNPs. n=3.

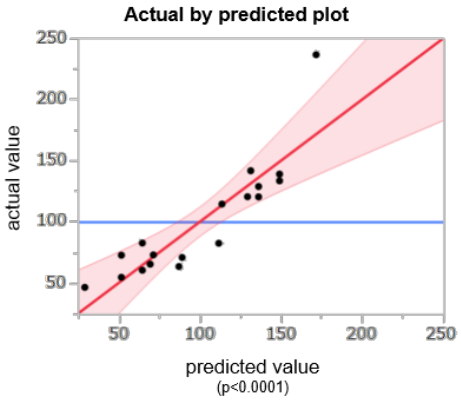

Summary of Fit	
R^2	0.785
Adjusted R^2	0.739
Root Mean Square Error	23.82
Mean	100.3
n	18

ANOVA Results			
Source	Degrees of Freedom	Sum of Squares	Mean Square
Model	3	29078.518	9692.84
Error	14	7943.508	567.39
Total	17	37022.026	

F-Test Results		
	F Ratio	Prob > F
ANOVA	17.0831	< 0.0001

Parameter Estimates				
Term in Model	Estimate	Std. Error	t Ratio	Prob > |t|
Intercept	107.74546	21.12533	5.10	0.0002
%PEG	-35.51921	12.83628	-2.77	0.0151
NaCl conc.	0.3527201	0.053484	6.59	< 0.0001
PL[DOPC]	11.293891	5.70573	1.98	0.0678

Effect Tests			
Effect	Sum of Squares	F Ratio	Prob > F
%PEG	4344.429	7.6568	0.0151
NaCl conc.	24676.815	43.3915	< 0.0001
PL	2223.049	3.9180	0.0678

Figure S8. Statistical information regarding the effective design-based model selection for definitive screening design to predict the ζ-average of the siRNA-loaded LNPs (C1 to C18).

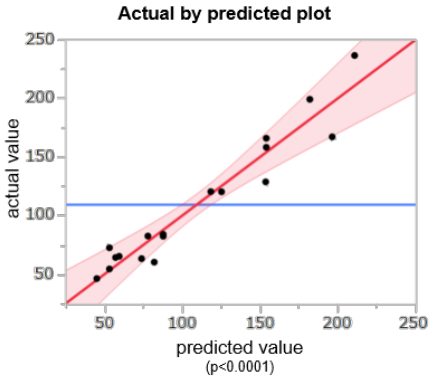

Summary of Fit	
R^2	0.929
Adjusted R^2	0.900
Root Mean Square Error	17.66
Mean	109.598
n	18

ANOVA Results			
Source	Degrees of Freedom	Sum of Squares	Mean Square
Model	5	49128.639	9824.73
Error	12	3740.612	311.72
Total	17	52869.251	
F-Test Results			
	F Ratio	Prob > F	
ANOVA	31.5212	< 0.0001	

Parameter Estimates				
Term in Model	Estimate	Std. Error	t Ratio	Prob > |t|
Intercept	-6.88206	29.34432	-0.23	0.8185
%CL	1.624419	0.471864	3.44	0.0049
NaCl conc.	0.4358821	0.039322	11.08	< 0.0001
%PEG	-28.81571	9.437277	-3.05	0.0100
(%CL-50)*(NaCl conc.-130)	0.0101418	0.004247	2.39	0.0343
(NaCl conc.-130)*(NaCl conc.-130)	0.0019481	0.000695	2.80	0.0160

Effect Tests			
Effect	Sum of Squares	F Ratio	Prob > F
%CL	3694.232	11.8512	0.0049
NaCl conc.	38302.638	122.8761	< 0.0001
%PEG	2906.209	9.3232	0.0100
(%CL-50)*(NaCl conc.-130)	1777.339	5.7018	0.0343
(NaCl conc.-130)*(NaCl conc.-130)	2448.221	7.8540	0.0160

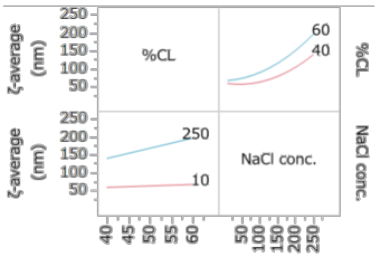

Figure S9. Statistical information regarding the effective design-based model selection for definitive screening design for predicting the ζ-average of the siRNA-loaded LNPs (C1 to C9, and C19 to C27).

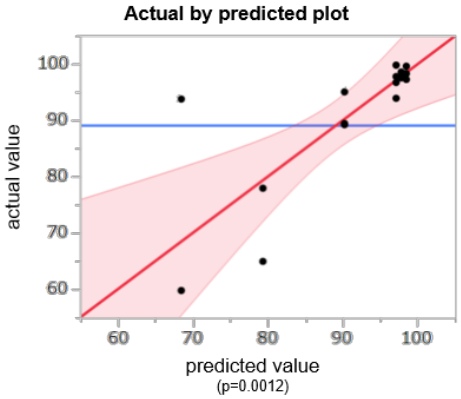

Summary of Fit	
R^2	0.667
Adjusted R^2	0.595
Root Mean Square Error	8.760
Mean	89.14
n	18

ANOVA Results			
Source	Degrees of Freedom	Sum of Squares	Mean Square
Model	3	2149.6190	716.540
Error	14	1074.2937	76.735
Total	17	3223.9127	

F-Test Results		
	F Ratio	Prob > F
ANOVA	9.3378	0.0012

Parameter Estimates				
Term in Model	Estimate	Std. Error	t Ratio	Prob > |t|
Intercept	88.574801	2.081305	42.56	< 0.0001
PL[DOPE]	9.2347016	2.081305	4.44	0.0006
NaCl conc.(10,250)	-5.788547	2.359978	-2.45	0.0279
PL[DOPE]*NaCl conc.(10,250)	5.1067149	2.359978	2.16	0.0483

Effect Tests			
Effect	Sum of Squares	F Ratio	Prob > F
PL	1510.6692	19.6868	0.0006
NaCl conc.(10,250)	461.6558	6.0162	0.0279
PL*NaCl conc.	359.3043	4.6824	0.0483

Figure S10. Statistical information regarding the effective design-based model selection for definitive screening design for predicting the percentage of siRNA encapsulation of the siRNA-loaded LNPs (C1 to C18).

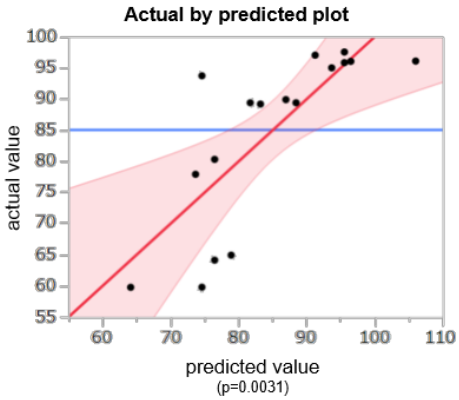

Summary of Fit	
R^2	0.617
Adjusted R^2	0.534
Root Mean Square Error	9.396
Mean	85.09
n	18

ANOVA Results			
Source	Degrees of Freedom	Sum of Squares	Mean Square
Model	3	1987.0488	662.350
Error	14	1235.9010	88.279
Total	17	3222.9498	

F-Test Results		
	F Ratio	Prob > F
ANOVA	7.5029	0.0031

Parameter Estimates				
Term in Model	Estimate	Std. Error	t Ratio	Prob > |t|
Intercept	79.701042	8.332767	9.56	< 0.0001
NaCl conc.	-0.079658	0.021097	-3.78	0.0020
PL[DSPC]	-6.184813	2.250593	-2.75	0.0157
%PEG	10.496464	5.063196	2.07	0.0571

Effect Tests			
Effect	Sum of Squares	F Ratio	Prob > F
NaCl conc.	1258.5840	14.2569	0.0020
PL	666.6763	7.5520	0.0157
%PEG	379.3955	4.2977	0.0571

Figure S11. Statistical information regarding the effective design-based model selection for definitive screening design for predicting the percentage of siRNA encapsulation of the siRNA-loaded LNPs (C1 to C9, and C19 to C27).

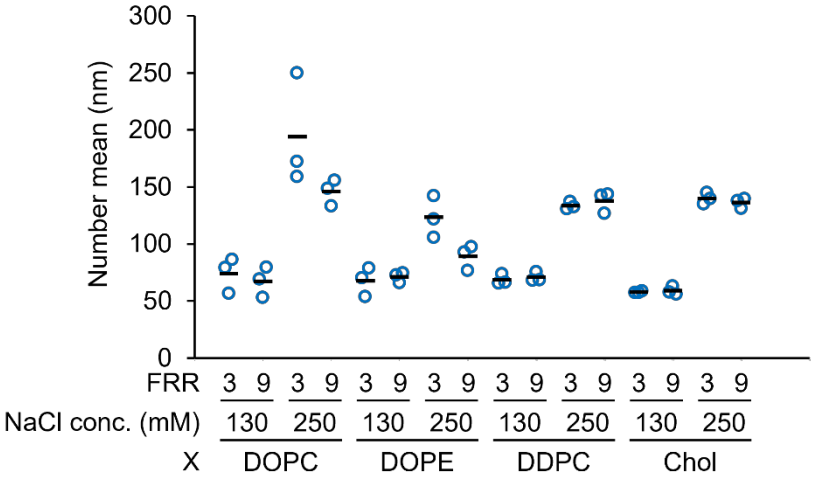

Figure S12. Number-weighted mean diameter of siRNA-loaded LNPs (related to Figure 4).

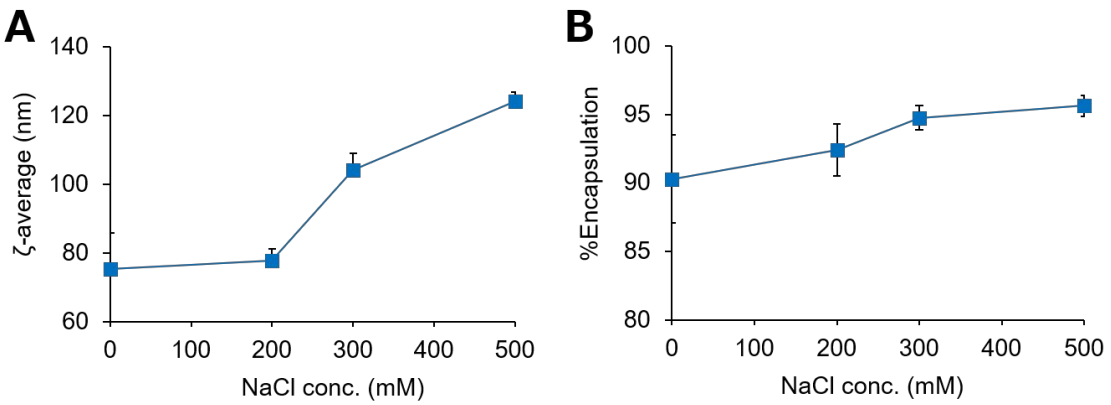

Figure S13. Effect of NaCl concentraion on the physicochemical properties of the siRNA-loaded YSK05-LNPs. (A, B) ζ-Average (A) and percentage of siRNA encapsulation (B) of the LNPs. n=3-4.

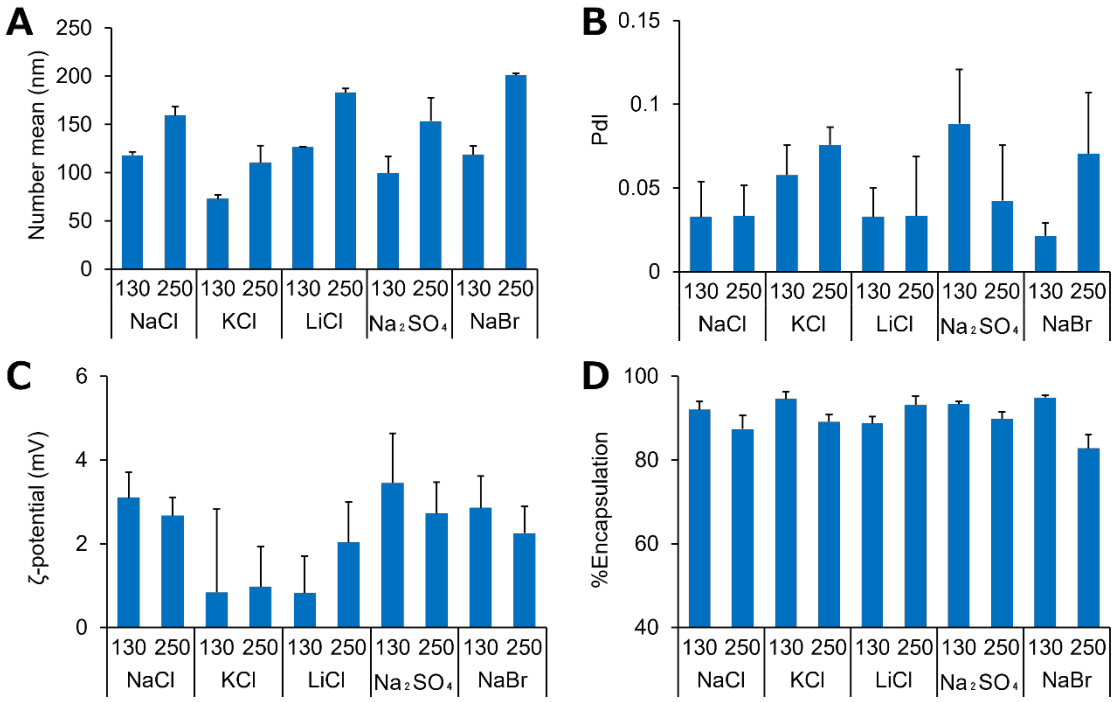

Figure S14. Physicochemical properties of siRNA-loaded LNPs synthesized with different types of and concentrations of salts. (A-D) Number mean (A), PdI (B), ζ-potential (C), and percentage of siRNA encapsulation (D) of the LNPs. n=3.